Volume 9
Number 45
7 December 2021
Pages 16047–16326

Journal of Materials Chemistry C

Materials for optical, magnetic and electronic devices

rsc.li/materials-c

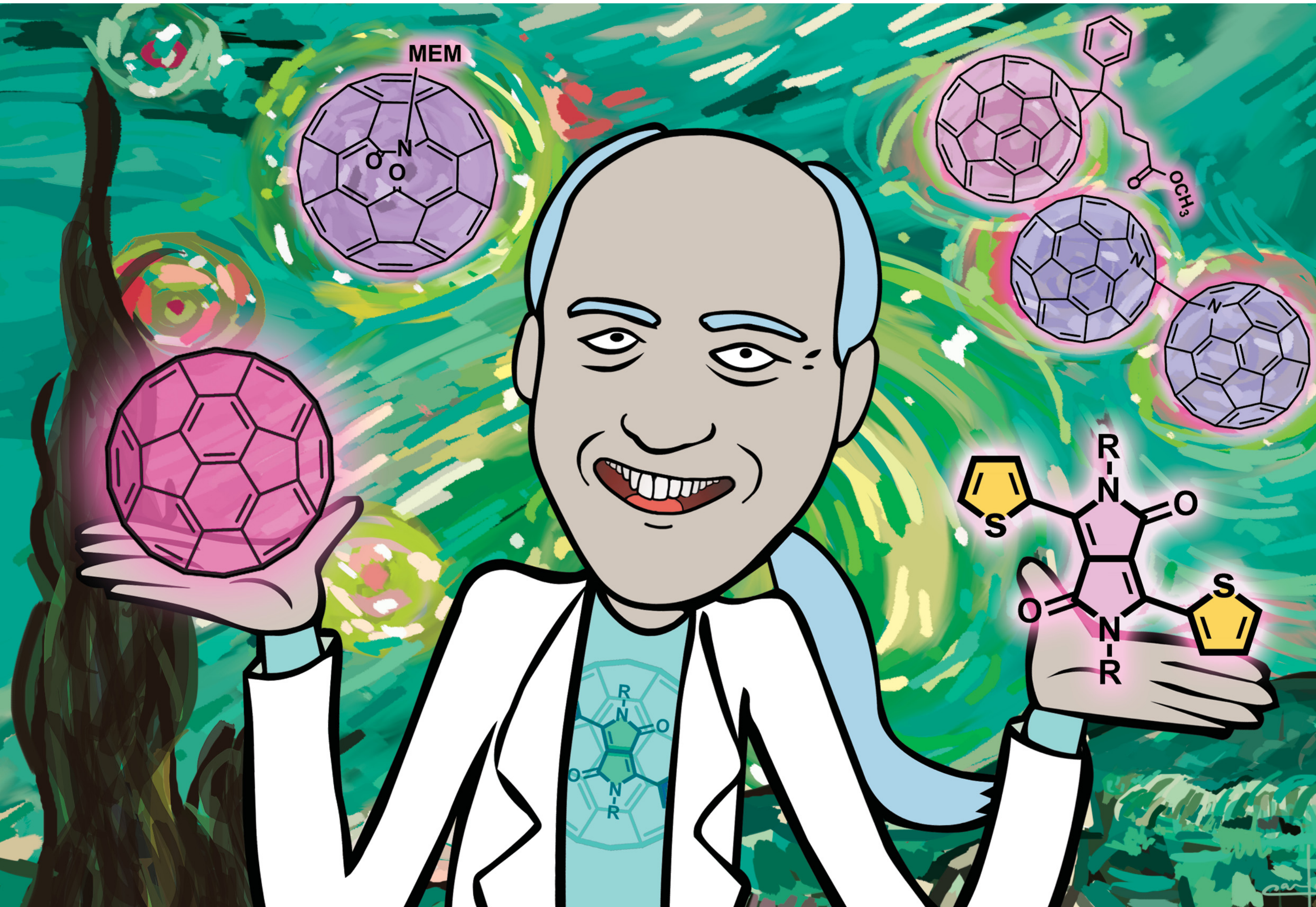

Special issue in honour of Kees Hummelen

ISSN 2050-7526

ROYAL SOCIETY OF CHEMISTRY

REVIEW ARTICLE
Ángela Sastre-Santos *et al.*
Diketopyrrolopyrrole-based single molecules in photovoltaic technologies

Journal of
Materials Chemistry C

REVIEW

View Article Online
View Journal | View Issue

Cite this: J. Mater. Chem. C, 2021, 9, 16078

Diketopyrrolopyrrole-based single molecules in photovoltaic technologies

Desiré Molina, Maria João Álvaro-Martins and Ángela Sastre-Santos *

Received 22nd April 2021, Accepted 19th July 2021

DOI: 10.1039/d1tc01872h

rsc.li/materials-c

The increasing demand for efficient energy sources has led to the emergence of photovoltaic (PV) technologies. However, there remains a need to move them from the laboratory scale to the general market, which requires exceptional materials that provide both stability and efficiency. Among the materials currently being investigated, diketopyrrolopyrroles (DPPs) stand out due to their chemical versatility, robustness, and optoelectronic properties, especially their intense absorption in the visible and near infrared spectrum, high charge carrier mobility in conjugated systems, good crystallinity and, sometimes, low production costs. In this article, we review the most successful DPP-based single molecules applied in emerging PV technologies to date. Thus, DPP single molecules applied in organic solar cells, dye-sensitized solar cells and perovskite solar cells are presented, together with their chemical structures, photovoltaic device performance and additional information. In addition, we attempt to give some pointers for the optimization of future, DPP-containing molecular designs and to highlight the potential of these building blocks.

1. Introduction

Organic semiconducting materials are essential for improving photovoltaic technologies as their optoelectronic properties can be tuned by modifying their chemical structure, thus allowing device performance to be optimized. In order to determine the most suitable such materials, a great deal of research effort has been exerted over the years. In this sense, there are many structures on which these novel materials are based, including porphyrinoids,[1,2] phthalocyanines,[3] perylenediimides,[4,5] and diketopyrrolopyrroles (DPPs).[6] The latter are a good example of moieties that can be used to build promising semiconductors.[7–10] DPPs were discovered in the 1970s by Farmum *et al.* as a by-product of the classical Reformatsky reaction between benzonitrile and ethyl bromoacetate.[11] DPPs are π-electron bicyclic-dilactam systems that act as electron acceptors. These derivatives are characterized by excellent stability, low solubility, and an intense red colour due to the extended π-conjugation between their electron-rich and electron-deficient units, as well as strong

Área de Química Orgánica, Instituto de Bioingeniería, Universidad Miguel Hernández, 03202 Elche, Spain. E-mail: asastre@umh.es

Desiré Molina

Desiré Molina is assistant professor of Organic Chemistry at Universidad Miguel Hernández de Elche. She received her PhD degree from Universidad Miguel Hernández de Elche in 2016, under the guidance of Prof. Ángela Sastre-Santos, where she has remained so far. She also joined the group of Prof. Anders Hagfeldt at EPFL (Switzerland) for 12 months as a postdoctoral fellow. Her research interests concern in the development of new materials for their application in photovoltaic technologies and other electrical devices.

Maria João Álvaro-Martins

Maria João Álvaro-Martins received her bachelor degree (2015) and master degree (2017) in chemistry from the Universidade de Lisboa. She is currently PH.D. student in Prof. Ángela Sastre-Santos research group at Universidad Miguel Hernández. Her research is focused on synthesis and characterization of diketopyrrolopyrroles derivatives for their aplication in photovoltaic devices.

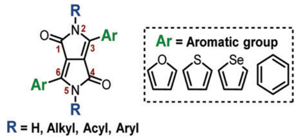

Fig. 1 General structure of DPPs and numbering of their atoms.

excitonic coupling in the solid state.[12,13] As such, DPPs started to be used as pigments. Due to the chemical versatility of DPPs, it was possible to synthesize other derivatives, which resulted in improvements and innovations in the pigment sector and, subsequently, in the plastics and inks industries.[14] Thus, it was observed that the optoelectronic properties could be varied by changing the chemical structure of DPP, thus allowing this type of compound to be used in a large number of applications. These systems can exhibit n-type, p-type or ambipolar semiconductor behaviour and can therefore provide the desired electronic character.[15] The 2,5-positions of the lactam nitrogens (Fig. 1) can be replaced by several groups, the most common being aryl, acyl and alky groups. These substitutions allow the solubility in organic solvents to be increased, whereas substitutions of the end-capping groups at the 3,6-positions perturbs the optoelectronic properties.[16,17] These end-capping groups can be different aromatic groups, depending on the reagents of origin of the DPPs (Fig. 1). Other appealing properties of DPP derivatives are their intense absorption in the visible and near infrared spectrum, their high charge-carrier mobility in conjugated systems, good crystallinity and low-cost production. In addition, DPPs can show high thermal, photochemical and mechanical stability.[10–19] The poor electronic character of the DPP core endows them with outstanding light-harvesting properties, while their flat structure enables significant intermolecular π–π interactions that facilitate charge mobility in organic field-effect transistors (OFETs).[20,21] As such, they are attractive building blocks with wide-ranging applications, especially in the field of photovoltaic technologies and OFETs.[18,22–27] In addition to these properties, DPPs also exhibit high fluorescence quantum yields in solution and in film, with a large extinction coefficient, which allows them to be used as fluorescence sensors.[28–34] Singlet fission has also been described in DPP systems, both in the solid state and in solution.[35,36] This property would allow the theoretical Shockley–Queisser limit to be increased from 32% to 45%, thus increasing the efficiencies of the solar devices in which they are integrated. Given the interesting properties of this type of compounds, many examples of DPP-based materials can be found in the literature, both single-molecule and polymers.[9–37] Single molecules have advantages over their polymeric counterparts because of their well-defined chemical structure, easier synthesis, lower batch-to-batch variation and high open-circuit voltage.[38,39] In this review article we recapitulate and discuss the latest advances in photovoltaics involving DPP-based single molecules, with an emphasis on the chemical structure of DPP-based systems, to gain an insight into the possible relationships between structure and performance in those devices in which they are integrated.

Ángela Sastre-Santos

Ángela Sastre-Santos is Full Professor of Organic Chemistry (2010) and Director of the Instituto de Bioingeniería at the Universidad Miguel Hernández de Elche (2019, Spain). She studied chemistry at the Universidad Autónoma de Madrid, where she obtained her PhD (1995, Tomás Torres). She was Postdoctoral fellow at the École Supérieure de Physique et Chimie Industrielles (Paris, Jacques Simon) and at the University of California, Santa Barbara and Los Angeles (Fred Wudl). She moved in 1998 to the UMH. Her research interest focuses on the synthesis of molecular and supramolecular electroactive systems with nano- and biotechnological applications.

2. DPP-based single molecules in organic solar cells

Organic solar cells (OSCs) have attracted a great deal of attention owing to their potential for obtaining lightweight and low-cost solar cells.[40] Various types of OSCs are discussed herein and classified into two general groups: planar (PHJ) (Fig. 2a) and bulk heterojunction (BHJ) OSCs (Fig. 2b and 3c). Both are structurally defined by a multilayer in which each layer can be deposited using a different manufacturing technique. In a typical OCS device, the active layer is composed of a bilayer (PHJ), or a blend of the donor and acceptor counterparts (BHJ), between an anode (generally ITO) and a metal electrode (cathode).[41] Interfacial layers, such as the hole-transport layer (HTL) and the electron-transport layer (ETL), are inserted between anode-photoactive and cathode-photoactive interfaces, respectively, to improve the performance and stability of the OSCs.[42] To simplify the model, it is assumed that the donor absorbs the light, then an electron is excited from the donor's highest occupied molecular orbital (HOMO) to its lowest unoccupied molecular orbital (LUMO). The resulting charge transfer is efficient if the offset between the donor LUMO and acceptor LUMO is high enough to overcome the exciton biding energy, which is typically 0.1–1.4 eV, thus giving rise to electron–hole pairs or excitons. In other words, the excitons must diffuse to the donor–acceptor interface, where there is enough potential energy drop to separate these excitons into the free charge carriers, namely electrons and holes (Fig. 2-i).[43] These electrons and holes are then transported to the respective electrode *via* the bicontinuous pathway, thereby avoiding recombination and charge capture. In this process, losses due to thermalization, absorption losses owing to spectral incompatibility, insufficient energy required for exciton splitting, *i.e.* $E_{\text{photon}} < E_{\text{band}}$ gap, which promotes a new state,

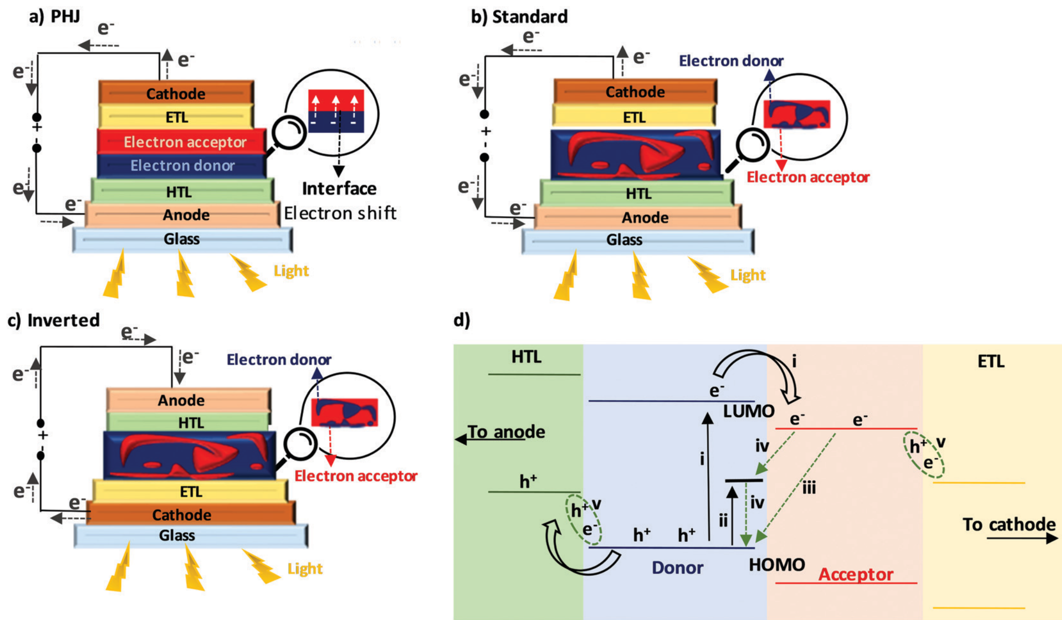

Fig. 2 General structure of: (a) a PHJ cell, (b) a standard BHJ, (c) an inverted BHJ and (d) general energy diagram of the photoelectric events involved in the operation of a standard OSC. (i) Excitation of an electron between donor HOMO–LUMO and the respective diffusion from the donor LUMO to acceptor LUMO ($E_{photon} > E_{band\ gap}$). (ii) The electron at the donor HOMO level absorbs a low-energy photon, thus promoting a new state and trapping the electron in this state. Recombination pathways are represented by downwards arrows and the green circle, where (iii) represents band-to-band recombination, (iv) trap-mediated recombination and (v) interfacial recombination.

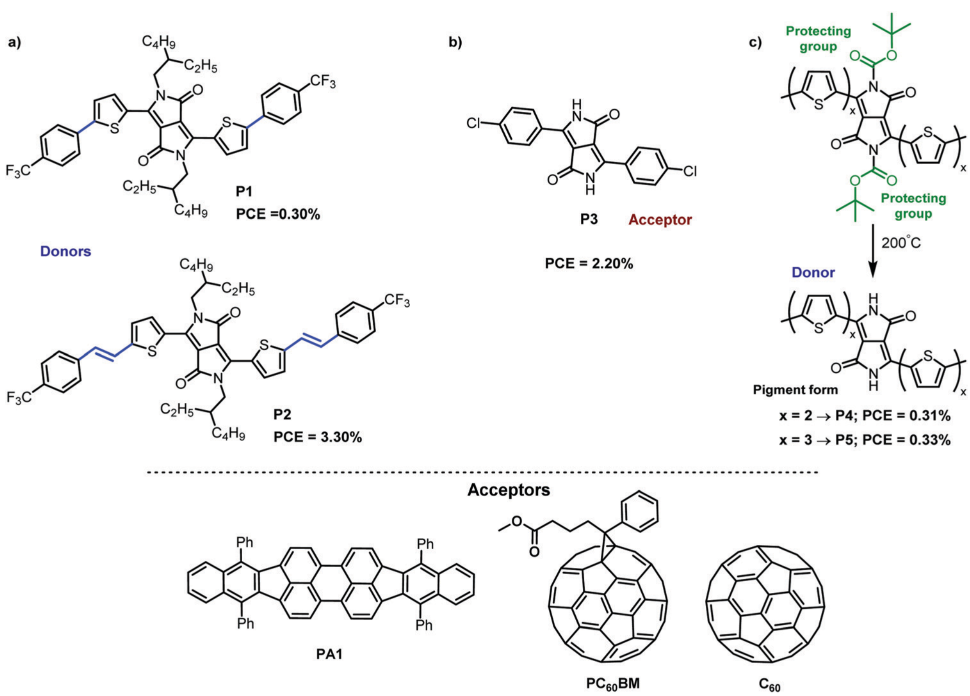

Fig. 3 Chemical structures and PCEs for (a) **P1** and **P2**, (b) **P3**, (c) **P4** and **P5**, and the acceptors PA1, $PC_{60}BM$ and C_{60}.

trapping the electron in this state (Fig. 2-ii), and charge recombination, can occur (Fig. 2iii–v).[44] As such, a low band gap material can improve device performance.[45] Over the past few years, an inverted device architecture has also been established for OSCs exhibiting a relatively high environmental stability. In an inverted device, the cathode is at the bottom while the top electrode is the anode (Fig. 2c).

Traditionally, given their excellent charge-transport performance, the electron–acceptor materials that have been extensively used in organic photovoltaics are fullerene acceptors (FAs). Representative examples include [6,6]-phenyl-C_{61}/C_{71}-butyric acid methyl ester ($PC_{60}BM$/$PC_{70}BM$) and indene-C_{60}/C_{70} bisadducts (ICBAs). These FAs have the disadvantage of being expensive and having electronic levels that are difficult to modify, in addition to poor absorption in the visible region. In contrast, non-fullerene acceptors (NFAs) are often energetically tunable by way of simple chemical modifications, thus allowing them to participate in light absorption and charge dissociation. Additionally, NFAs can provide longer device lifetimes since they usually present greater thermo- and photostability. In fact, in recent years there has been a marked improvement in single-molecule-based NFAs, many of which now exceed power conversion efficiencies (PCEs) of 15%,[46,47] and very recently there was a quantitative leap to PCEs as high as 18.2%.[48,49] DPP-based single molecules are presented below, illustrating their chemical structure (both donor and acceptor); the structures of their non-DPP counterparts can be found in the corresponding section.

2.1. DPP-based single molecules in PHJs

PHJs were first reported in 1986 by Tang. These devices are based on two layers stacked on top of each other. Each layer comprises different organic films, one with a donor moiety and the other with an acceptor semiconductor (Fig. 2).[50] In these devices, only excitons generated at a distance of 10–20 nm from the interface can reach the heterojunction. Under these conditions, the efficiency of the resulting solar cells is limited by the charge generation. In addition, the photovoltaic properties are strongly dependent on the nature of the electrodes. Although a lot of scientific work had already been published on this topic,[51,52] the first example of DPP-based single molecules in PHJs would not be published until 2011. In this article, Kylberg *et al.* described the application of two DPP derivatives end-capped with two trifluoromethylphenyl groups (**P1** and **P2**) together with C_{60} (Fig. 3) as the acceptor counterpart.[53] **P2** contained extra vinylene bridges between the aromatic rings (Fig. 3a). The best performance was obtained with this latter after thermal annealing (PCE = 3.30%, short-circuit current density (J_{sc}) = 7.89 mA cm^{-2}, open-circuit voltage (V_{oc}) = 790 mV and fill factor (FF) = 53%, under AM 1.5G illumination (100 mW cm^{-2})). However, as a maximum PCE of 0.3% was achieved with **P1**, the structure with the most extended conjugation could be more advantageous. These derivatives were also used as electron acceptors in BHJ.[54] Peng *et al.* designed an NFA PHJ solar cell using tetraphenyldibenzoperiflanthene (PA1, Fig. 3) as the donor and a 4-chlorophenyl-DPP (**P3**) as the acceptor (Fig. 3b). This work aimed to compare the results for the PHJ and a planar-mixed heterojunction solar cell (PM-HJ). PM-HJ devices contain a layer between the donor and acceptor layers. This architecture increases the exciton photogeneration, maintaining a high V_{oc} and FF.[55] With the PM-HJ architecture glass/ITO/MoO_3/PA1/PA1:**P3**/**P3**/BCP/Ag they obtained a better performance (PCE = 3.20%) than with the regular PHJ one, mainly because of the improvement in J_{SC} from 2.78 to 5.42 mA cm^{-2}, despite presenting both lower V_{oc} and FF. This donor/acceptor interface suggests a high interface energy gap and a relatively low saturation, thus highlighting the importance of these two parameters to generate a high V_{oc}. In a recent study, Rooney *et al.*, synthesized two DPP-based latent pigment donor materials (**P4** and **P5**, Fig. 3c). Latent pigments are organic pigments with a chemically or thermally removable functionality, which induces a non-permanent dye-type solubility.[56] Di-*tert*-butyl dicarbonate (*t*-BOC) protecting groups were introduced at the lactam nitrogens as this sterically bulky group can prevent the formation of π–π stacking networks and H-bonding sites, thereby the improving the solubility in common organic solvents. Once deposited, the protecting groups were removed thermally at 200 °C. These materials were combined with $PC_{60}BM$ (Fig. 3) as acceptor in an ITO/PEDOT:PSS/DDP-DPP-Donor/$PC_{60}BM$/ETL/Al architecture.[57] The best performance was obtained for **P5** after thermal annealing of the entire device at 140 °C using LiF as ETL (J_{sc} = 2.11 mA cm^{-2}, V_{oc} = 375 mV, FF = 42.6%, PCE = 0.33%). As we will see below, DPP-based PHJ OSCs performed more poorly than their BHJ OSC analogues.

2.2. DPP-based single molecules in BHJs

DPP-based single molecules have been widely used in BHJ OSC devices and applied in a variety of structures. DPPs can form part of the structure of both donor single molecules and acceptor single molecules, thereby emphasizing their versatility.

2.2.1. DPP-based single molecules as donors in BHJs. DPP-based single donor molecules will be classified here as linear donor molecules with a DPP core, linear donor molecules with a core flanked by DPPs, star-shaped DPP-based donor molecules and donor molecules based on porphyrinoids and DPPs.

2.2.1.1. Linear donor molecules with a DPP core. These molecules have a central DPP core with different substituents attached to the aromatic rings at positions 3 and 6 of the diketopyrrolopyrrole bicycle. Due to the electronic nature of their component units, these systems are usually of the donor–acceptor–donor (D–A–D) type, with DPP being the acceptor. Since this structure induces intramolecular charge transfer, these materials absorb over a greater range of the spectrum and at longer wavelengths. Furthermore, by changing groups D and A, the photophysical properties of these systems can be tuned.[58] Numerous relevant studies have been published in this regard. For instance, Patil *et al.* published two papers in 2016 in which they describe both symmetrical (**BH1** and **BH3**) and asymmetric (**BH2** and **BH4**) narrow band gap molecules, whose flanks were arranged triphenylamines (TPAs) (**BH1** and **BH2**)[59] or *N*-phenyl carbazoles (**BH3** and **BH4**),[60] linked *via* an ethyne moiety (Fig. 4a). Using $PC_{70}BM$ (Fig. 4) as the acceptor material, these authors obtained better results with those derivatives containing carbazole moieties after surface treatment with a methanol/acetonitrile (98 : 2) blend. Thus, **BH4** showed a PCE of 5.73% *vs.* 5.31% for **BH2**, while **BH3** gave a PCE of 4.65% *vs.* 4.06% for **BH1**. As such, better results were obtained with an asymmetrical structure including a carbazole heterocycle. The same authors reported a symmetrical D–π–A–π–D dipolar donor single molecule based on the donor moiety ferrocene also linked to the DPP core *via* an ethynyl bridge (**BH5**, Fig. 4b). The optimal ITO/PEDOT:PSS/**BH5**:$PC_{70}BM$/PFN/Al device with DIO additive gave rise to a PCE of up to 6.44% with a high J_{sc} of 10.48 mA cm^{-2}, a V_{oc} of 940 mV and an FF of 64% after thermal

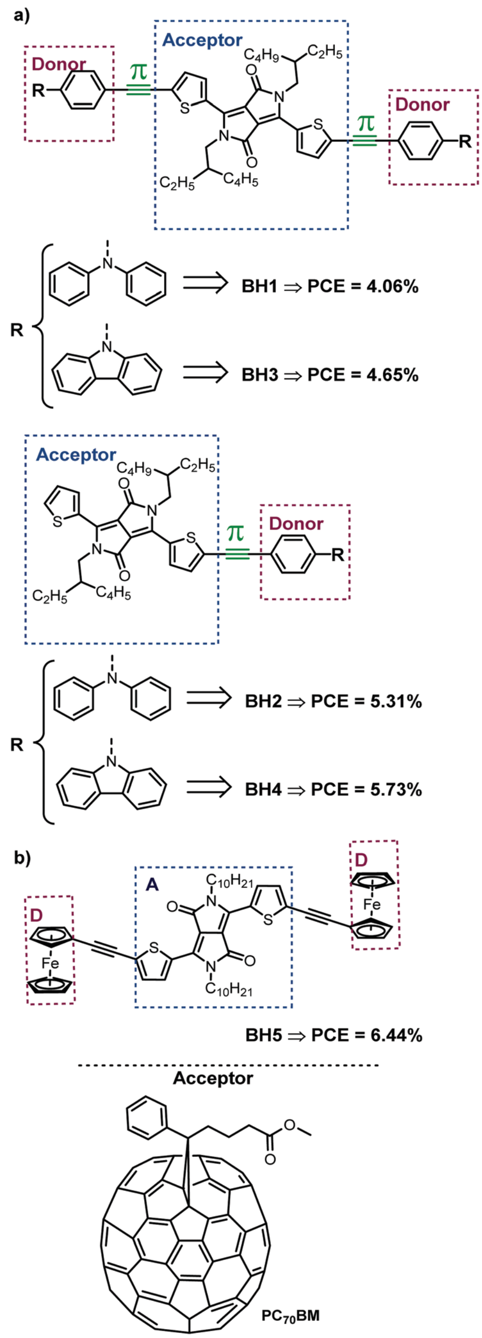

Fig. 4 Chemical structures and PCEs of the donors **BH1–BH5** and the acceptor $PC_{70}BM$.

annealing.[61,62] These studies show that inclusion of the ethynyl bridge leads to a lower HOMO, and therefore to a higher V_{oc}, as well as enhanced intermolecular π–π stacking, thus facilitating intramolecular charge transport (Table 1).

2.2.1.2. Linear donor molecules with a core flanked by DPPs. These structures include a central core, usually of an aromatic nature, linked and also more or less conjugated to the DPP moieties. Most of these systems present an A–D–A molecular structure in which the acceptor moieties are usually the DPPs. As these systems of an electronic push–pull nature, their optoelectronic properties are also customizable as in the previous group and, of course, there are numerous publications in this field. For example, Shi *et al.* developed a DPP–fluorene–DPP derivative (**BH6**, Fig. 5a) as the donor and the acceptor materials in BHJ OSCs together with the counterparts $PC_{70}BM$ and P3HT (Fig. 5), respectively, on both devices, thus demonstrating the ambipolar capacity of the DPP moiety. In this section we will focus on **BH6** as donor. To evaluate the electron donor potential of **BH6**, devices with the architecture ITO/PEDOT:PSS/**BH6**:$PC_{70}BM$/PFN/Al were manufactured. The best PV performances were obtained with a donor/acceptor ratio of 1 : 3, with a PCE of 3.26% measured under AM 1.5G illumination (100 mW cm^{-2}) (Table 2).[63] The same year, a DPP-dithienopyran (DTP)-DPP system was presented by Jung *et al.* (**BH7**, Fig. 5b). **BH7** was tested as donor with $PC_{70}BM$ and the n-type NFA conjugated polymer N2200 (Fig. 5). These authors performed their study with the inverted architecture ITO/ZnO/active layer/MoO_3/Ag, testing different donor/acceptor ratios. The best efficiencies were obtained with $PC_{70}BM$ when a 1 : 3 donor/acceptor ratio was used (PCE of 6.88%), while the best device performance with N2200 **BH7**/N2200 (1 : 2) was 4.82%, mainly because J_{sc} and FF were lower in the latter case (Table 2).[64] Similarly, Tang *et al.* described a single molecule with a large hole mobility based on DPP-thieno[2,3-*f*]benzofuran (TBF)-DPP (**BH8**, Fig. 5c). The device architecture ITO/PEDOT:PSS/**BH8**:Acceptor/LiF/Al was used, comparing the photovoltaic performance of devices fabricated with PCBM and with the NFA N2200. The devices with N2200 as the acceptor gave better results than those with FA. The device that worked best contained a donor/acceptor ratio of 1 : 3 and 1-chloronaphthalene (CN) as solvent additive. The PCE for N2200 was 3.74%, and the best PCE for **BH8**/PCBM was 3.44% (Table 2).[65]

To investigate the new NFAs SdiPBI and SdiPBI-S (Fig. 5) in BHJ OSCs, Feng *et al.* coupled them to a narrow bandgap donor DPP-pentacyclic bislactam-DPP (**BH9**, Fig. 5d). SdiPBI and SdiPBI-S derivatives had a complementary absorption (400–600 nm) to **BH9**.

Table 1 Acceptor, band gap, LUMO, additive, architecture, and PV parameters for linear donor molecules with a DPP-core single molecule

Donor	Acceptor	LUMO (eV)	Band gap (eV)	Additive	Architecture[a]	J_{sc} (mA cm^{-2})	V_{oc} (mV)	FF (%)	PCE (%)	Ref.
BH1	$PC_{70}BM$	−3.77	1.72	DIO	Standard	11.16	850	56	4.06	59
BH2	$PC_{70}BM$	−3.69	1.84	DIO	Standard	8.88	880	52	5.31	59
BH3	$PC_{70}BM$	−3.60	1.73	Methanol/acetonitrile (98 : 2)	Standard	8.19	980	58	4.65	60
BH4	$PC_{70}BM$	−3.64	1.90	Methanol/acetonitrile (98 : 2)	Standard	9.58	980	61	5.73	60
BH5	$PC_{70}BM$	−3.64	1.58	DIO	Standard	10.48	940	64	6.44	61 and 62

[a] No additives were used.

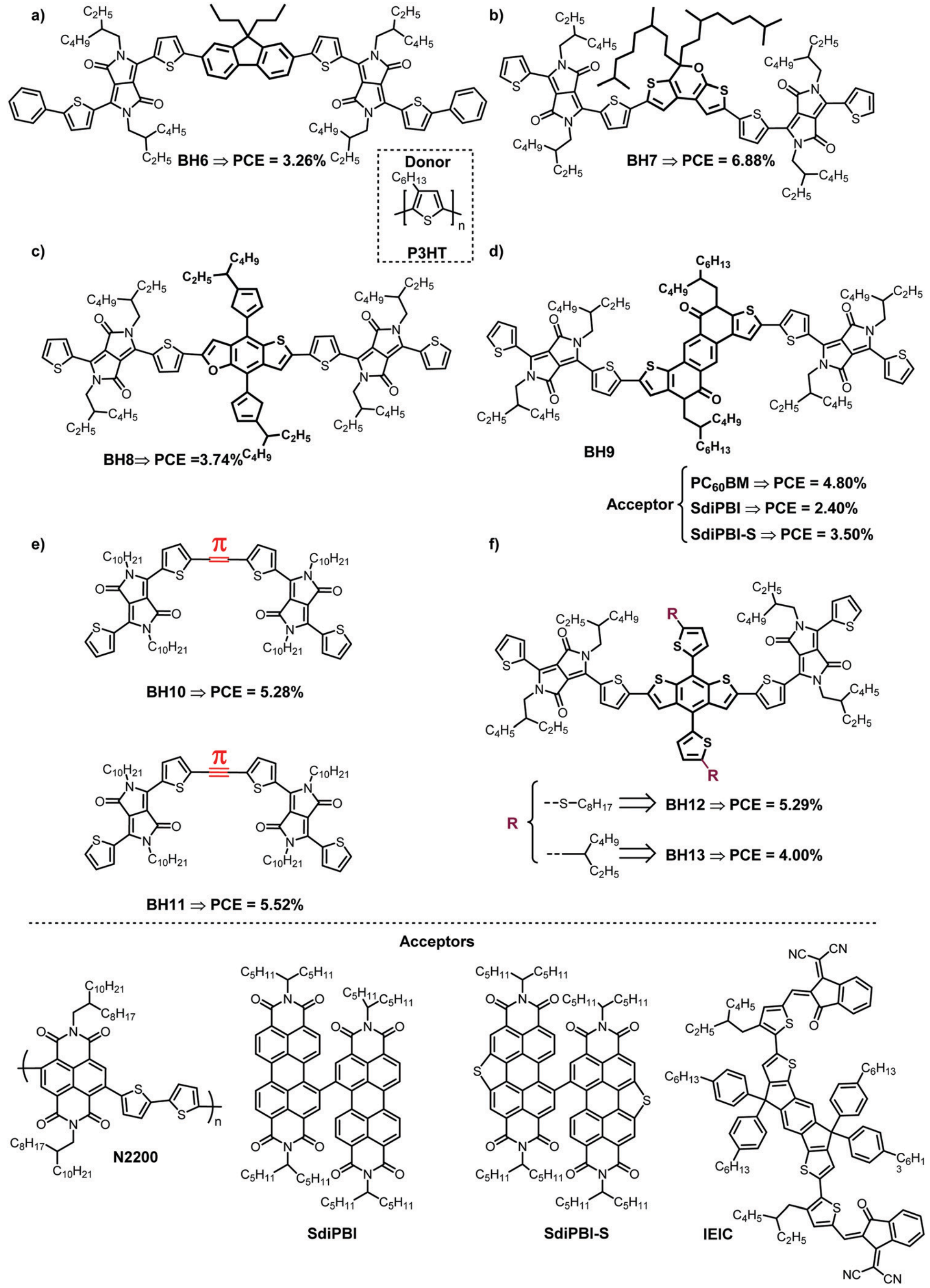

Fig. 5 Chemical structures and PCEs for the DPP-core-DPP donors **BH6-BH13**, the donor P3HT and the acceptors N2200, SdiPBI and SdiPBI-S.

After an optimization process using the standard architecture ITO/PEDOT:PSS/Active layer/LiF/Al, **BH9**:$PC_{60}BM$ provided the best PCE of 4.80%, while the non-fullerene solar cells also exhibited promising PCEs of 2.40% and 3.50% (Table 2). The relatively low carrier mobilities of these NFAs and the large phase separation could be responsible for the lower efficiency of these solar cells.[66] An interesting study in which the synthesis of two DPP-based single molecules having the structure D–A–D–π–D–A–D was described was published by Patil *et al.* The difference was the bridge connecting the two DPP units, which was either a double or a triple bond (**BH10** and **BH11**, respectively; Fig. 5e). This work highlights the utility of thermal and solvent annealing treatments in improving the performance of organic devices. The authors described how, after these treatments, the efficiencies improved from 1.98% and 1.85% to 5.28% and 5.52% for **BH10** and **BH11**, respectively (Table 2).[67] Lin *et al.* compared two donors based on a DPP-benzo[1,2-*b*:4,5-*b*′]dithiophene (BDT)-DPP (**BH12** and **BH13**, Fig. 5f). **BH12** had linear alkylthio substituents in the thiophene units of the BDT moiety, whereas **BH13** presented alkyl chains in these positions. As a consequence, significant variations in crystallinity, phase separation, charge transport and photovoltaic properties were

Table 2 Acceptor, band gap, LUMO, additive, architecture, and PV parameters for DPP-core-DPP donor single molecules

Donor	Acceptor	LUMO (eV)	Band gap (eV)	Additive	Architecture	J_{sc} (mA cm^{-2})	V_{oc} (mV)	FF (%)	PCE (%)	Ref.
BH6	$PC_{70}BM$	−3.39	1.82	Annealed at 120 °C	Standard	8.08	890	45	3.26	63
BH7	$PC_{70}BM$	−3.73	1.52	—	Inverted	14.12	800	61	6.88	64
BH7	N2200				Inverted	10.14	820	58	4.82	
BH8	$PC_{70}BM$	−3.50		CN	Standard	8.20	740	56	3.44	65
BH8	N2200					7.60	820	60	3.74	
BH9	$PC_{60}BM$	−3.73	1.65	$CHCl_3$/DIO	Standard	9.70	890	56	4.80	66
BH9	SdiPBI					6.10	920	42	2.40	
BH9	SdiPBI-S					6.70	960	53	3.50	
BH10	$PC_{70}BM$	−3.47	1.54	TSA	Standard	11.53	790	58	5.28	67
BH11	$PC_{70}BM$	−3.45	1.62	TSA	Standard	10.82	910	56	5.52	67
BH12	IEIC	−3.49	1.79	$CHCl_3$/*o*-DCB	Standard	9.80	930	58	5.29	68
BH12					Inverted	10.87	940	59	6.03	
BH13	IEIC	−3.46	1.77	$CHCl_3$/*o*-DCB	Standard	8.24	900	54	4.00	68
BH14	$PC_{60}BM$	−3.46	1.58	—	Standard	10.92	828	61	5.53	69
BH14	IDIC					10.16	811	58	4.80	
BH15	$PC_{60}BM$	−3.43	1.64	—	Standard	7.32	830	57	3.48	69
BH15	IDIC					11.30	820	59	5.48	
BH16	ITIC	−3.67	1.67	$CHCl_3$/DIO	Inverted	13.35	850	63	7.15	70

No additives were used. TSA – two step annealing.

observed, and **BH12** showed higher hole mobility (1.1×10^{-2} cm^2 V^{-1} s^{-1}) than **BH13** (3.0×10^{-3} cm^2 V^{-1} s^{-1}). **BH12** and **BH13** were subsequently applied as a donor semiconductor together with IEIC (Fig. 5) as NFA in the active layer. The best results were obtained using a binary solvent ($CHCl_3$ and *o*-dichlorobenzene [*o*-DCB]) with the device architecture ITO/PEDOT:PSS/active layer/Ca/Al. The binary solvent leads to appropriate phase separation domain sizes, higher domain purity, better charge transport properties and better photovoltaic performance of the blended films. **BH12**-containing devices demonstrated better PV performance, with a PCE of 5.29%, while **BH13**-containing devices achieved a PCE of 4.00%. Finally, when **BH12** was included in inverted architecture devices, all photovoltaic parameters were improved, reaching an efficiency of 6.03% (J_{sc} of 10.87 mA cm^{-2}, V_{oc} of 940 mV and FF of 59%).[68] In 2018, Huo *et al.* developed two DPP-based donor materials compatible with both FA and NFA (2,2′-((2*Z*,2′*Z*)-((4,4,9,9-tetrahexyl-4,9-dihydro-*s*-indaceno[1,2-*b*:5,6-*b*′]dithiophene-2,7-diyl)bis(methanylylidene))bis(3-oxo-2,3-dihydro-1*H*-indene-2,1-diylidene))dimalononitrile) (IDIC, Fig. 6). The structure of these materials follows the same scheme as we have seen previously: two DPP units flanking a BDT donor unit. On this occasion, the intention was to determine the effect of two aromatic substituents with different degrees of conjugation extension (**BH14**, with a bithiophene group and **BH15**, with an (*E*)-1,2-di(thiophen-2-yl)ethane group, Fig. 6a). BHJ devices had the architecture ITO/PEDOT:PSS/Active layer/PDIN/Al

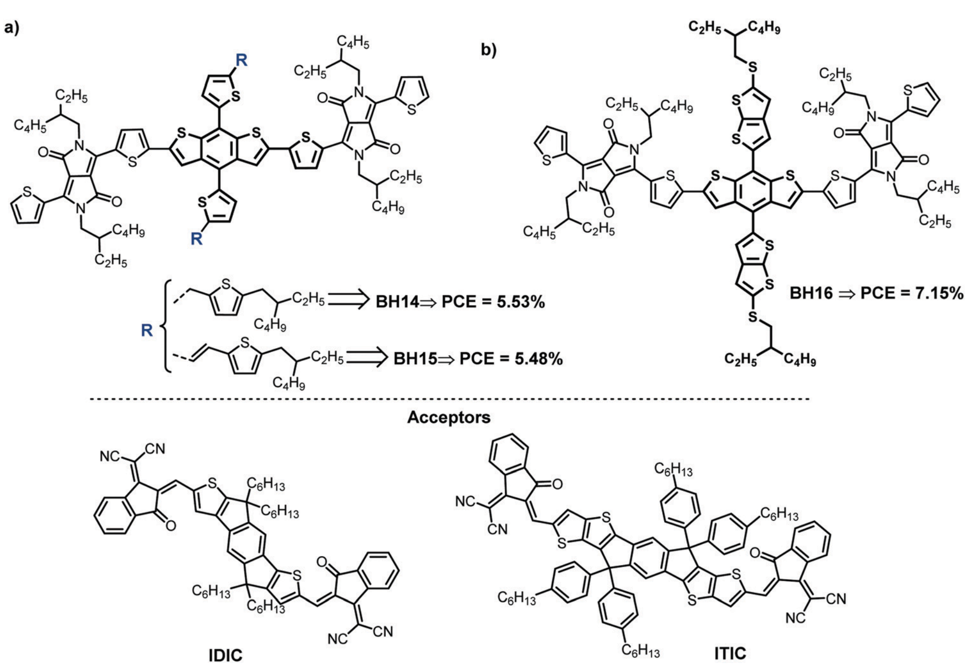

Fig. 6 Chemical structures and PCEs for the DPP-core-DPP donors **BH14–BH16** and the acceptors IDIC and ITC.

(where PDIN is *N,N′*-bis(propylenedimethylamine)-3,4,9,10-perylenediimide, the cathode interfacial layer). The acceptors with which they were studied were the FA $PC_{60}BM$ and the NFA IDIC (Fig. 6a). The best PV results for **BH14** were obtained with the FA (PCE = 5.53%, J_{sc} = 10.92 mA cm^{-2}, V_{oc} = 828 mV and FF = 61%), while for **BH15** they were obtained with the NFA (PCE = 5.48%). The authors attribute these differences mainly to the higher absorptions of the active layers when mixtures **BH14**:$PC_{60}BM$ and **BH15**:IDIC are used *versus* **BH14**:IDIC and **BH15**:$PC_{60}BM$, which led to a higher J_{sc}.[69] Jung subsequently studied **BH14** against other acceptors such as $PC_{70}BM$ and 3,9-bis(2-methylene-(3-(1,1-dicyanomethylene)-indanone)-5,5,11,11-tetrakis(4-hexylphenyl)-dithieno[2,3-*d*:2′,3′-*d*′]-*s*-indaceno[1,2-*b*:5,6-*b*′]dithiophene) (ITIC, Fig. 6) with the architecture ITO/ZnO/**BH14**: acceptor/MoO_3/Ag. In order to extend the conjugation length in two-dimensions, in 2019 Jung *et al.* attached a 5-alkylthio-thieno[3,2-*b*]thiophene unit to the central BDT moiety (**BH16**, Fig. 6b). **BH16** exhibited a strong intermolecular interaction in the solid state, an intense UV-vis absorption with a band gap of 1.71 eV, well matched energy levels with those of the NFA ITIC, and also good crystallinity in the film state. The best **BH16**:ITIC devices showed an overall PCE of 7.15% This result was one of the best for single molecules in non-fullerene BHJ OSCs.[70]

2.2.1.3. Star-shaped DPP-based donor molecules. Star-shaped molecules are trimers, tetramers, pentamers, *etc.*, whose constituent units are linked to a central nucleus and usually conjugated. This type of system has advantages over its linear counterparts, such as higher solubility, better film formation and less optical anisotropy properties.[71]

A series of star-shaped acceptor–acceptor–donor (A–A–D) compounds based on a triazine core, 2,5-thienyl DPP or 1,4-phenylene DPP as the π-conjugated bridge and *tert*-butyl-substituted triphenylamine (*t*TPA) and *tert*-butyl-substituted carbazole (*t*Cz) as end groups and donor units were synthesized by Shiau *et al.* in 2015 (Fig. 7a and Table 3). These three donors were combined with the FAs $PC_{60}BM$ and $PC_{70}BM$ as acceptor materials. **BH17** gave the best performance, exhibiting higher parameters than the other two systems when $PC_{60}BM$ was the acceptor (a PCE of 1.08% for **BH17** *versus* 0.79% for **BH18** and 0.24% for **BH19**). These differences in the photovoltaic performance were due to the fact that charge transfer between *t*TPA and 2,5-thienyl DPP in the compound **BH17** is higher than for **BH18** and **BH19**. Additionally, the lower band-gap and broader solar-light absorption favor photo-energy conversion. When the acceptor material was changed to $PC_{70}BM$, it was possible to improve the efficiencies in the devices fabricated with the same optimized conditions as for $PC_{60}BM$ (PCEs of 1.57%, 1.14% and 0.39% for **BH17**, **BH18** and **BH19**, respectively).[72]

Liu *et al.* designed two novel DPP-based 3D molecular donors (**BH20** and **BH21**, Fig. 7b and Table 3). The FA $PC_{70}BM$ and the NFA N2200 were also compared in the inverted architecture ITO/ZnO/active layer/MoO_3/Ag. After optimization of the active layer composition and adding CN, BH20 gave rise to PCEs of 3.56% and 4.64% with $PC_{70}BM$ and N2200, respectively, and BH21 yielded values of 4.02% and 3.22%, respectively. These differences in **BH20**/acceptor devices were due to the fact that the mixtures with N2200 generated higher quantum efficiencies than those based on $PC_{70}BM$, as evidenced by the incident photon to current efficiency (IPCE).[73]

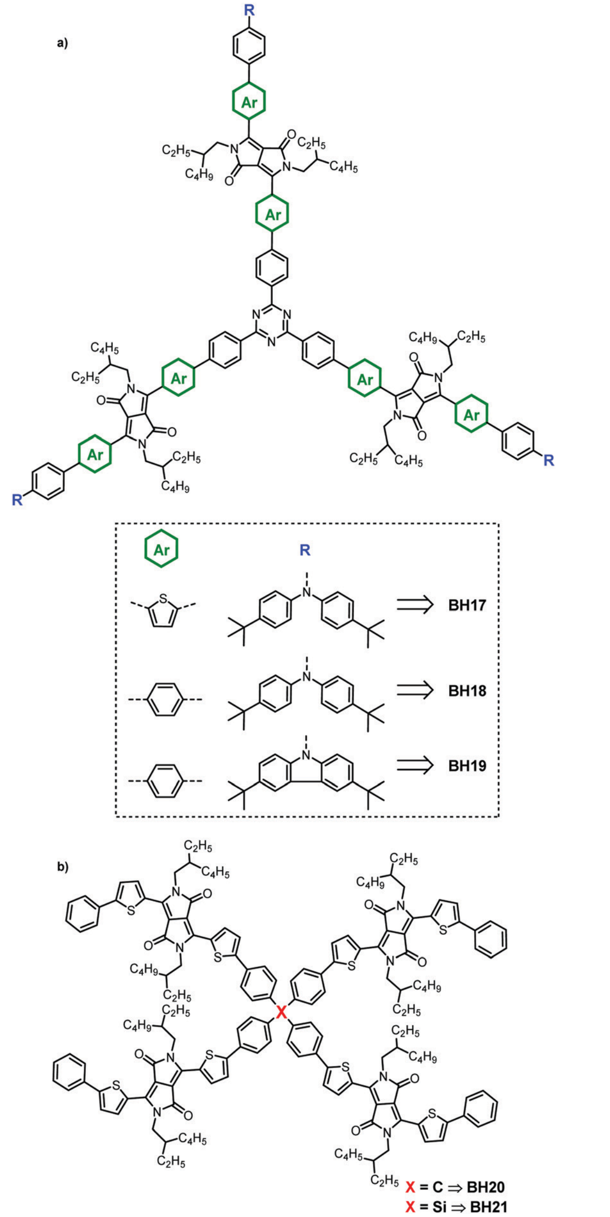

Fig. 7 Chemical structures for the star-shaped donors **BH17–BH21**.

2.2.1.4. Donor molecules based on porphyrinoids and DPPs. One very successful approach has involved the combination of DPP moieties with porphyrinoid (Por) macrocycles[74] to obtain efficient donors, which is why these systems have been given their own subsection. Thus, Liang *et al.* synthesized tetrafuranyl and a tetraselenyl DPP-Por-DPP systems using triple bonds as connectors between the units (**BH22** and **BH23**, Fig. 8a). The aim of this work was to determine how the different chalcogen atoms influence the PV performance of the devices by comparing these

Table 3 Acceptor, LUMO, band gap, additive, architecture, and PV parameters for star-shaped DPP and DPP-Por donor single molecules **BH17–BH36**

Donor	Acceptor	LUMO (eV)	Band gap (eV)	Additive	Architecture	J_{sc} (mA cm^{-2})	V_{oc} (mV)	FF (%)	PCE (%)	Ref.
BH17	$PC_{60}BM$	−3.68	1.58	—	Standard	4.81	700	32	1.08	72
	$PC_{70}BM$			—		6.34	730	34	1.57	
BH18	$PC_{60}BM$	−3.41	2.06	—	Standard	4.63	550	31	0.79	72
	$PC_{70}BM$			—		5.85	610	62	1.14	
BH19	$PC_{60}BM$	−3.42	2.09	—	Standard	1.80	470	30	0.24	72
	$PC_{70}BM$			—		2.75	500	28	0.39	73
BH20	$PC_{70}BM$	−3.35	2.01	CF	Inverted	7.69	890	50	3.56	
	N2200			CF		8.59	870	52	4.64	
BH21	$PC_{70}BM$	−3.4	2.04	DIO	Inverted	7.12	860	49	3.22	73
	N2200			DIO		8.14	890	54	4.02	
BH22	$PC_{60}BM$	−3.55	1.38	Pyridine	Standard	10.52	810	50	4.26	75
BH23	$PC_{60}BM$	−3.61	1.33	DIO	Standard	14.93	710	55	5.81	75
BH24	$PC_{60}BM$	−3.60	1.36	DIO	Standard	16.00	710	64	7.23	76
BH25	$PC_{70}BM$	−3.74	1.52	—	Standard	12.43	880	61	6.67	77
BH26	$PC_{70}BM$	−3.79	1.44	—	Standard	14.32	950	67	8.98	77
BH27	IDIC	−3.85	1.37	TA	Inverted	15.46	710	56	6.13	78
BH28	IDIC	−3.86	1.37	TA	Inverted	14.03	710	53	5.21	78
BH29	IDIC	−3.87	1.41	TA	Inverted	11.46	700	51	4.08	78
BH30	6TIC	−3.81	1.37	DIO+ SVA	Standard	20.44	800	74	12.08	79–81
BH31	$PC_{70}BM$	−3.90	1.40	SVA	Standard	15.98	890	66	9.24	82
BH32	$PC_{70}BM$	−3.72	1.72	SVA	Standard	14.31	820	62	7.27	82
BH33	IDT-C8	−3.51	1.30	SVA	Standard	11.15	710	65	5.14	83
BH34	Y6	−3.24	1.82	CN + TA	Standard	16.88	780	52	6.86	84
BH35	Y6	−3.33	2.02	DIO + TA	Standard	18.26	690	55	6.93	84
BH36	$PC_{70}BM$	−3.33	1.57	—	Inverted	5.00	551	38	1.04	85

No additives were used. TA – thermal annealing treatment. SVA – solvent vapor annealing.

two molecules with a previously described tetrathienyl analogue (**BH24**, Fig. 8a) in the standard architecture ITO/PEDOT:PSS/donor:$PC_{60}BM$/PFN/Al.[75] **BH23** gave better PV parameters than **BH22** when 0.6% DIO was added (PCE of 5.81%, J_{sc} of 14.93 mA cm^{-2}, V_{oc} of 710 mV and FF of 55%; Table 3), although it was possible to significantly improve the performance of **BH22** by replacing the DIO with 1 vol% of pyridine (PCE of 4.26%, J_{sc} of 10.52 mA cm^{-2}, V_{oc} of 810 mV and FF of 50%). Nevertheless, **BH24** continued to hold the series record with a PCE of 7.23%. The active layer containing **BH23** presents a more favorable morphology than for **BH22**, although **BH24** provides a better morphology than either, with a smaller downhill driving force for electron transfer and exciton dissociation.[76] A further interesting example is the work of Bucher *et al.*, who designed and synthesized two single molecules comprising a boron-dipyrromethene (BODIPY) core linked to two Por by phenyl (**BH25**) or thienyl units (**BH26**) and also linked to two DPP units (Fig. 8b). The BHJ devices were designed using the following architecture: ITO/PEDOT:PSS/donor:$PC_{70}BM$/PFN/Al. Upon optimization of the active layer after solvent vapor annealing, **BH26** reached a PCE of 8.98% (J_{sc} of 14.32 mA cm^{-2}, V_{oc} of 950 mV and FF of 67%) *versus* a PCE of 6.67% for **BH25** (Table 3). The higher values for **BH26** could be related to better exciton dissociation, higher charge transport and charge mobility.[77]

The combination of DPP-Por donors with NFA has led to the best results in OSCs for single molecules based on DPP. Thus, Hadmojo *et al.* fabricated devices using three different NIR-absorbing porphyrin-DPP donors and an IDIC as acceptor (**BH27–BH29**, Fig. 8c). The influence of the meso substituents in the porphyrin (*p*-octoxyphenyl (**BH27**), *p*-(2-ethyl)-hexoxyphenyl (**BH28**) and 5-(2-ethyl)hexylthiophenyl groups (**BH29**)) was analyzed. After optimization of the active layer, **BH27**:IDIC gave a PCE of 6.13% (J_{sc} of 15.46 mA cm^{-2}, V_{oc} of 710 mV and FF of 56%), which was higher than for **BH28**:IDIC (PCE of 5.21%) and **BH29**:IDIC (PCE of 4.08%). The side chains on the porphyrin donors modified the nanomorphologies of the BHJ devices, thus giving better PCE values to the **BH27**-based devices due to the more face-on preferred donor and acceptor domains.[78] In 2019, Gao *et al.* presented the DPP-Por-DPP donor **BH30** (Fig. 8d), which was studied in fullerene-free BHJ OSCs in the standard architecture ITO/PEDOT:PSS/**BH30**:6TIC[79,80] (Fig. 9)/C_{60}-bissalt/Ag, where C_{60}-bissalt is the ETL. After applying a solvent annealing treatment and including DIO as additive, a record efficiency was achieved for non-tandem fullerene-free single molecule devices up to that date. The best device reached a PCE as high as 12.08% from a high J_{sc} of 20.44 mA cm^{-2}, a V_{oc} of 800 mV and an also high FF of 74% (Table 3).[81] More recently, Cuesta *et al.* compared two Por-DPP-Por systems. In **BH31**, the DPP core is flanked by separate selenophene rings, while in **BH32** these rings are replaced by thiophenes (Fig. 8e). The BHJ devices were fabricated with the conventional architecture glass/ITO/donor:$PC_{70}BM$/PFN/Al. After solvent vapor annealing, the best performance was achieved with an overall PCE value of 9.24% (J_{sc} of 15.98 mA cm^{-2}, V_{oc} of 890 mV and FF of 66%) and 7.27% (J_{sc} of 14.31 mA cm^{-2}, V_{oc} of 820 mV and FF of 62%) for **BH31** and **BH32**, respectively. The authors explained this difference based on the more planar conformation due to smaller lamellar stacking and π–π stacking distances, broader absorption spectrum and higher hole mobility of **BH31** compared to **BH32**, which led to a more favorable active layer morphology for exciton

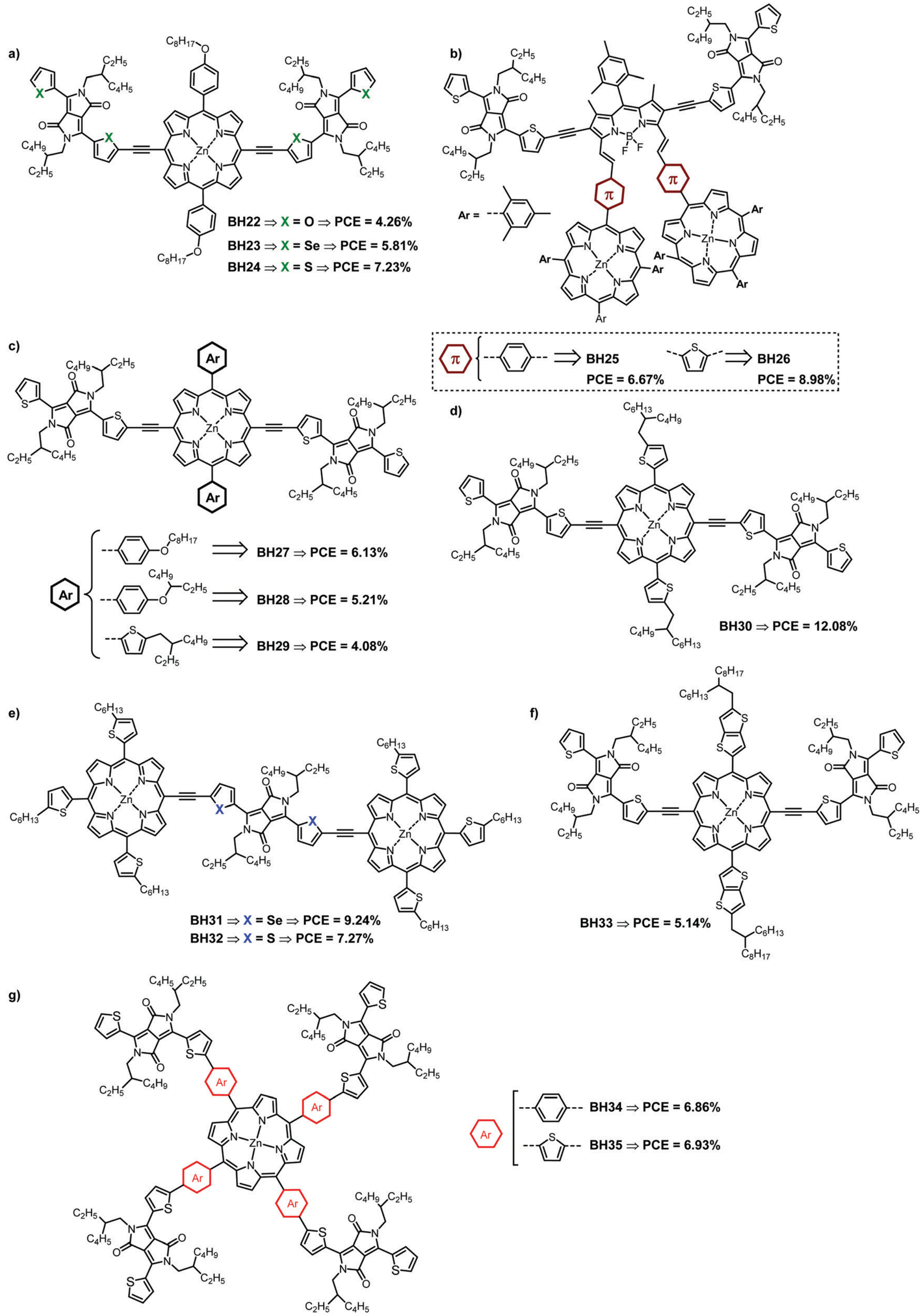

Fig. 8 Chemical structures and PCEs for the DPP-Por donors **BH22–BH35**.

dissociation and charge transport.[82] Chen *et al.* presented a thieno[3,2-*b*]thiophene-functionalized DPP-Por-DPP structure (**BH33**, Fig. 8f), which formed part of the active layer together with the IDT-C8 acceptor. The PCE values for all small molecule OSCs increased from 0.64% to 5.14% after SVA for the standard architecture ITO/PEDOT:PSS/**BH33**:IDT-C8 (Fig. 9)/PDINO/Al,

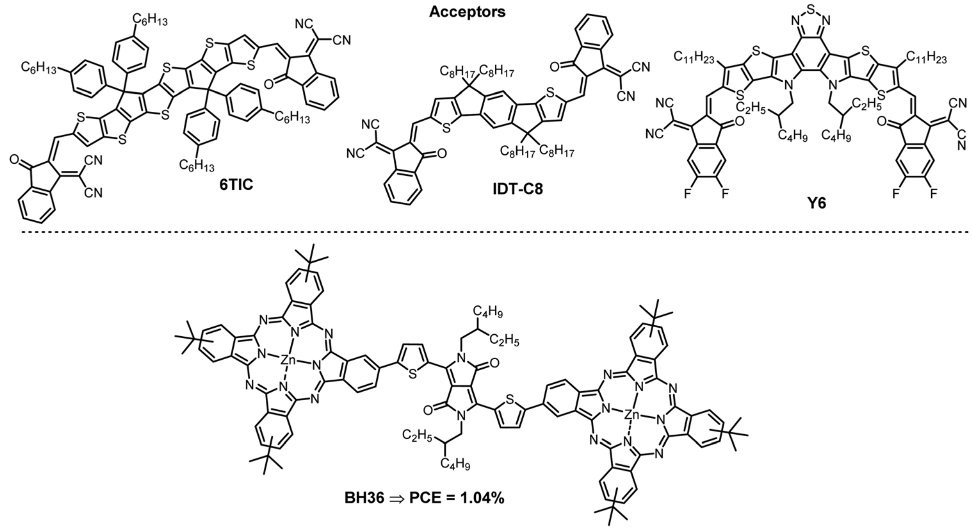

Fig. 9 Chemical structures and PCEs for the DPP-Pc donor **BH36** and the acceptors 6TIC, IDT-C8 and Y6.

where PDINO is (N,N'-bis(propylenedimethylamine)-3,4:9,10-perylenediimide).[83] Two star-shaped DPP-Por donors were presented very recently. Their structures include a central zinc-porphyrin with its four meso positions linked to each DPP unit *via* two different aromatic rings, namely phenyl (**BH34**) or thienyl (**BH35**) (Fig. 8g). These materials were studied as donors in OSCs with the acceptor Y6 (Fig. 9), with the standard architecture ITO/PEDOT:PSS/active layer/PDINO/Al. A maximum PCE of 6.86% was achieved with **BH34** when 0.75 vol% CN was used as solvent additive and after a thermal annealing at 120 °C for 10 minutes. **BH35** gave the best performance (PCE of 6.93%, J_{sc} of 18.26 mA cm^{-2}, V_{oc} of 690 mV and FF of 55%) using DIO as additive after a thermal annealing at 80 °C also for 10 minutes (Table 3). The geometry of both molecules was determined by theoretical calculations. A more orthogonal geometry was established for **BH35**. Moreover, it was found that DPP-arms were more coplanar with the thienyl linker for **BH35** than in the case of **BH34**. The small differences in performances were attributed to these geometric characteristics, thus suggesting that the orthogonal geometry of **BH35** favors the formation of additional charge pathways.[84]

Other well-known porphyrinoids include phthalocyanines (Pcs). Molina *et al.* published a study presenting a Pc–DPP–Pc conjugate system (**BH36**, Fig. 9) as donor in the standard architecture glass/ITO/HTL/**BH36**:PC$_{70}$BM/Ca/Ag, where HTL was PEDOT:PSS or MoO$_3$. The best results were obtained with MoO$_3$ as HTL (PCE = 1.04%, J_{sc} of 5.00 mA cm^{-2}, V_{oc} of 551 mV and FF of 38%), since PEDOT:PSS was able to protonate the donor, thus worsening the interface contact (Table 3).[85]

Considering the data described, the most successful approach for the design of DPP-donors is the one that includes a porphyrin in its structure. In this category, the stiffer molecules, which include triple bonds, give rise to the best photovoltaic parameters (**BH26**, **BH30**, and **BH31**, PCEs of 8.98%, 12.08% and 9.24%, respectively). In contrast, the 3D design of DPP-donors did not result in adequate morphologies, with a mean PCE of 2.07% and a maximum of 4.64% (**BH20**). Similarly, linear DPP-donor designs did not give significantly better results depending on the position of the DPP units (core or flanks). With regard to the acceptor counterparts, although there is less data, all PV parameters are higher, on average, when NFAs are used, including the above-mentioned **BH30**, which holds the record for this series.

2.2.2. DPP-based single molecules as acceptor material in BHJ. The current interest in developing NFAs has already been mentioned. In this regard, DPP acceptors are strong candidates for building acceptors for BHJ OSCs due to all the properties discussed above, especially their acceptor core formed by the bilactam and their ambipolar character. Sonar *et al.*[86] and Karsten *et al.*,[87] in 2010, were the pioneers in the field of using DPP derivatives as electron–acceptors, which opened the door to intensive research in this area. Analogously to donors, the acceptors will also be classified here according to their molecular structure as linear acceptor molecules with a DPP core, linear acceptor molecules with a core flanked by DPPs, star-shaped DPP-based acceptor molecules and spirofluorene-DPP-based acceptor molecules.

2.2.2.1. Linear acceptor molecules with a DPP core. The characteristics of these systems are similar to those for linear donor systems, although it is usual to find structures that combine DPPs with other electron-acceptor units, such as 1,1,4,4-tetracyanobuta-1,3-diene (TCBD), rhodanines (Rho) and perylenediimides (PDI).

TCBD is a strong electron-withdrawing unit that promotes charge transport and imparts good solubility in organic solvents due to its nonplanar structure. Patil *et al.* described various TCBD-DPP based compounds (**BH37–BH42**, Fig. 10a–f). For **BH37** (mono-substituted) and **BH38** (di-substituted), the TCBD was extended with triphenylamine (Fig. 10a and b). These single molecules exhibited a good thermal stability and a broad and strong absorption in the NIR region complementary to the conjugated polymer Pol-1 (Fig. 10). A PCE of 3.90% was obtained for **BH37**, and for **BH38** the PCE value was 4.95%.[88] In **BH39**

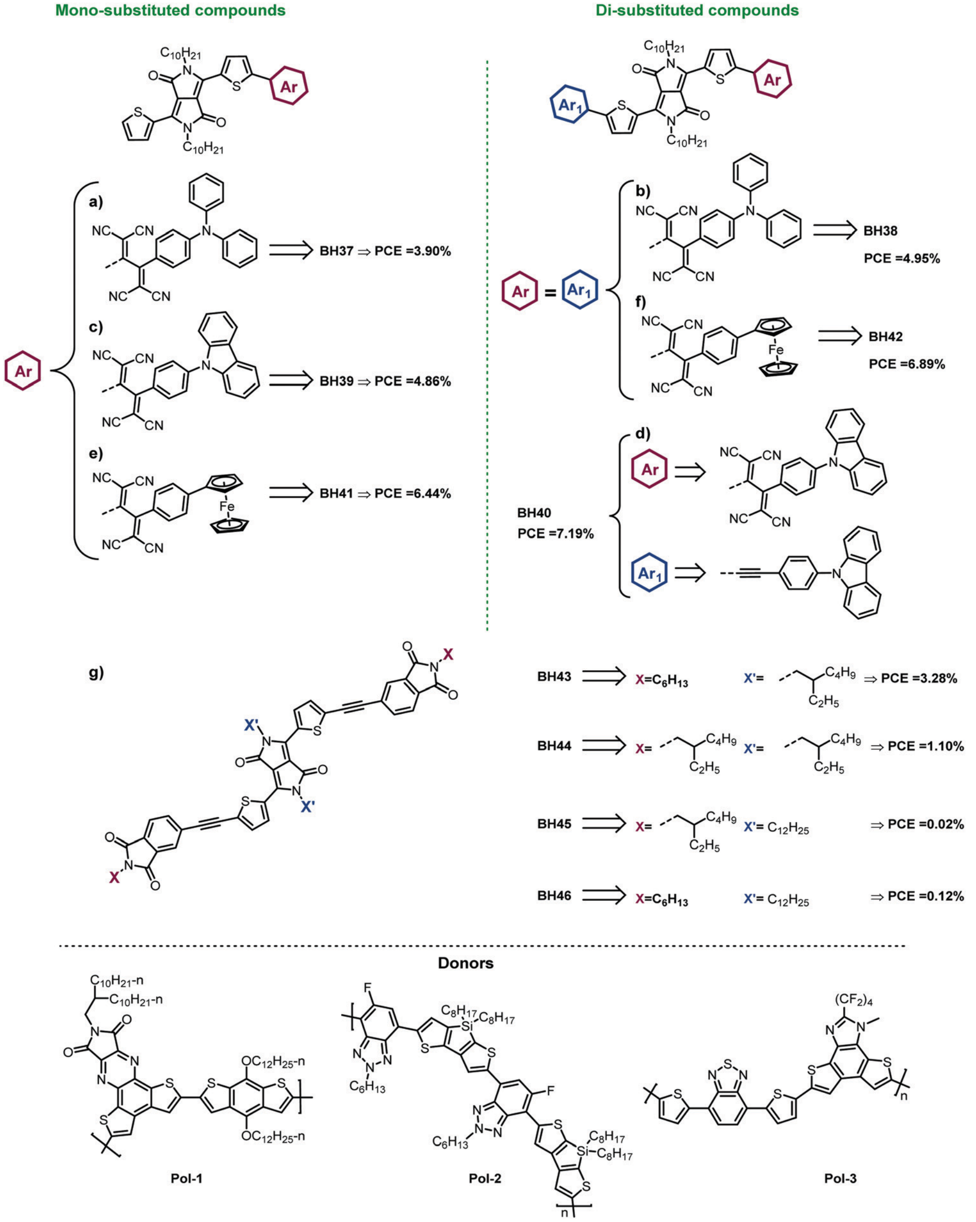

Fig. 10 Chemical structures and the best PCEs for the acceptors **BH37–BH46** and the donor polymers Pol-1, Pol-2, and Pol-3.

(mono-substituted) and **BH40**, *N*-phenylene carbazole (Fig. 10c and d) was used as end-group, with **BH40** being a disubstituted asymmetric compound with ethynylene-*N*-phenylene carbazole as the end group on one side and a TCBD-*N*-phenylene carbazole on the other.[89,90] After optimization of the devices using a thermal annealing treatment, the best PCEs were 4.86% and 7.19% for Pol-2:**BH39** and Pol-2:**BH40**, respectively (Fig. 10). These different values arise as a result of a large J_{sc} and FF for **BH40** (Table 4), related to the broader Pol-2:**BH40** absorption profile and more balanced charge transport. In turn, when these authors replaced carbazole with ferrocene to give **BH41** (mono-substituted) and **BH40** (di-substituted), the PCE values were similar (6.44% and 6.89% for Pol-3:**BH41** and Pol-3:**BH42**, respectively; Fig. 10e and f). According to the authors, the results obtained were similar due to the large values of J_{sc} and FF. Despite this, the J_{sc} and FF values for **BH42** are slightly higher than for **BH41** (Table 4)due to the better charge transport and lower lamellar and π–π stacking distance.[91]

Josse *et al.* designed and synthesized two materials based on phthamilides as end group with a thienoisoindigo and a DPP (**BH43**) bridged by acetylene moieties (Fig. 10g). The best performance for P3HT:**BH43** was obtained using the inverted cell architecture (ITO/ZnO/active layer/MoO_3/Ag), with DIO as solvent additive, and after a thermal annealing treatment. Thus, a PCE of 3.28% was obtained under these conditions.[92] The same group subsequently studied the influence of the alkyl side chain in this kind of compound on PV performance, using **BH43** as reference. The effects of the nature (linear or branched alkyl chain) and position (in the DPP and in the phthalimide) of the side chain on the optical properties and, consequently, the

Table 4 Donor, LUMO, band gap, additive, architecture, and PV parameters for linear DPP acceptor single molecules

Acceptor	Donor	LUMO (eV)	Band gap (eV)	Additive	Architecture	J_{sc} (mA cm^{-2})	V_{oc} (mV)	FF (%)	PCE (%)	Ref.
BH37	Pol-1	−4.22	1.32	SVA	Standard	8.15	920	52	3.90	89
BH38	Pol-1	−4.36	1.28	SVA	Standard	10.21	860	56	4.95	89
BH39	Pol-2	−3.83	1.69	SVA	Standard	10.56	940	49	4.86	90
BH40	Pol-2	−3.81	1.52	SVA	Standard	13.78	900	58	7.19	90
BH41	Pol-3	−3.92	1.51	VD	Standard	11.34	980	58	6.44	91
BH42	Pol-3	−4.02	1.37	VD	Standard	12.66	880	62	6.89	91
BH43	P3HT	−4.13	1.65	DIO	Inverted	5.91	890	50	3.28	92
BH44	P3HT	[a]	1.67	DIO	Inverted	4.40	500	40	1.10	93
BH45	P3HT	[a]	1.64	DIO	Inverted	0.51	140	25	0.02	93
BH46	P3HT	[a]	1.64	DIO	Inverted	2.72	150	25	0.12	93
BH47	P3HT	−3.79	1.49	TA	Standard	3.34	610	63	1.28	94
BH48	P3HT	−3.93	1.48	TA	Standard	2.06	750	31	0.49	94
BH49	P3HT	−4.17	1.52	TA	Standard	3.56	410	52	0.77	96
	DTS(QxHTh$_2$)$_2$	−3.99	1.85	SVA	Standard	11.04	1020	62	6.98	97
	Pol-2			DIO	Standard	12.37	980	62	7.52	97
BH50	DTS(QxHTh$_2$)$_2$	−4.15	1.57	SVA	Standard	12.15	940	68	7.76	97
BH51	*p*-DINI-(FBTTTh$_3$)$_2$	−3.74	1.87	SVA	Standard	13.72	980	67	9.14	98
BH52	PTB7-Th	−3.70	1.60	SVA	Inverted	10.84	970	44	4.63	99 and 100
BH53	SM1:PC$_{70}$BM	−3.96	1.64	SVA	Standard	16.32	920	67	10.05	101
BH54	P3HT	−3.65	1.66	DIO + TA	Standard	6.25	970	39	2.37	102
BH55	P3HT	−3.74	1.82	TA	Standard	3.16	1170	62	2.30	103
BH56	PTB7	−4.18	1.52	DCB+ CN	Inverted	7.77	830	47	3.03	104
BH57	PTB7	−4.33	1.52	DCB+ CN	Inverted	12.10	810	51	5.00	104

[a] Not reported. TA: thermal annealing. SVA: solvent vapor annealing. VD: vacuum dried.

corresponding PV performance, was studied. The UV-vis absorption spectra recorded for solutions and films showed two types of behavior: (1) compounds **BH43** and **BH44** (branched chains in DPP core) arranged to form J-aggregates in the solid state; and (2) compounds with linear side chains in the DPP core (**BH45** and **BH46**) formed H-aggregates. The authors concluded that the branched alkyl chain in the DPP favors light absorption and promotes a better phase separation with P3HT, whereas the linear chain in phthalimide improves the charge-transport properties. The efficiencies obtained this time were 1.10%, 0.02% and 0.12% for **BH44**, **BH45** and **BH46**, respectively.[93]

A series of A1–π–A2–π–A1 single molecules (**BH47–BH49**), in which a thiophene and/or furan were introduced between two strong electron-withdrawing units, namely DPP (A2) and Rho (A1) (Fig. 11a and b), was reported by Eom *et al.*[94] These authors applied these compounds as donors and acceptors in combination with PC$_{70}$BM and P3HT, respectively, due to their ambipolar character. The best performance was obtained with the architecture ITO/PEDOT:PSS/active layer/LiF/Al, where P3HT:**BH47** gave the highest PCE of 1.28%, exceeding the PCE obtained for **BH47**:PC$_{70}$BM (0.92%). A PCE of 1.77% was obtained for **BH48** when mixed with PC$_{70}$BM (1.77%), but only 0.49% for P3HT (Table 4). In contrast, in the case of **BH49**, higher parameters were achieved when this compound was used as the acceptor in the active layer along with P3HT (0.77%) than with PC$_{70}$BM (0.02%). When Privado *et al.* substituted the LiF by PFN and added DIO, the PCE for the P3HT:**BH49** mixture improved to 2.16%.[95] Likewise, the PCE increased to 4.17% when using Pol-2 as the donor, subsequently increasing up to 7.52% when DIO was added, with a J_{sc} of 12.37 mA cm^{-2}, a V_{oc} of 980 mV and an FF of 62% (Table 4). The higher PCE for Pol-2:**BH49** was related to the broader absorption profile of the active layer, low energy loss and balanced charge transport.[96] Subsequently, dicyano groups were introduced at the rhodanine moieties of the thiophene-DPP (**BH50**, Fig. 11b) by the same research group, who reported a comparative study between **BH49** and **BH50** as acceptors using DTS(QxHTh$_2$)$_2$ as donor counterpart. The best PCEs were obtained when the active layer was dried under vacuum (VD) instead of using the thermal annealing technique. The vacuum-dried active layer improved the FF by suppressing bimolecular recombination and enhancing charge transport. DTS(QxHTh$_2$)$_2$:**BH50** exhibited a PCE of 7.76% with a J_{sc} of 12.15 mA cm^{-2}, a V_{oc} of 940 mV and an FF of 68%, while for DTS(QxHTh$_2$)$_2$:**BH49** the best PCE was 6.98%. These results were attributed to the fact that **BH50** blends exhibited enhanced light absorption, molecular ordering and crystallinity.[97] As an evolution of this structure, the ethynyl linker was used as a bridge between the terminal dicyanorhodanine and the dithiophene-DPP core (**BH51**, Fig. 11c). In that study, *p*-DINI-(FBTTTh$_3$)$_2$ (Fig. 11) was used as donor because it presents good energy levels that match with the those of **BH51**. The SVA method was implemented again, obtaining a high PCE of 9.14% with a J_{sc} of 13.72 mA cm^{-2}, a V_{oc} of 980 mV and an FF of 67%, and this system currently holds the record for DPP-based single molecules as acceptors in OSCs (Table 4).[98]

Combination of the DPP core with *N*-annulated PDIs was described by the Welch group in two studies in which the **BH52** derivative (Fig. 11d) is combined with different donor polymers in the active layer (P3HT, PCDTBT, PTB7-Th and PDTT-BOBT), in the inverted architecture ITO/ZnO/Donor:**BH52**/MoO$_X$/Ag. Using the SVA processing method, PCEs of up to 4.63% with a J_{sc} of 10.84 mA cm^{-2}, a V_{oc} of 970 mV and an FF of 44% could be achieved with the donor PTB7-Th (Fig. 11 and Table 4). The donor polymer PDTT-BOBT also gave good PCEs (maximum

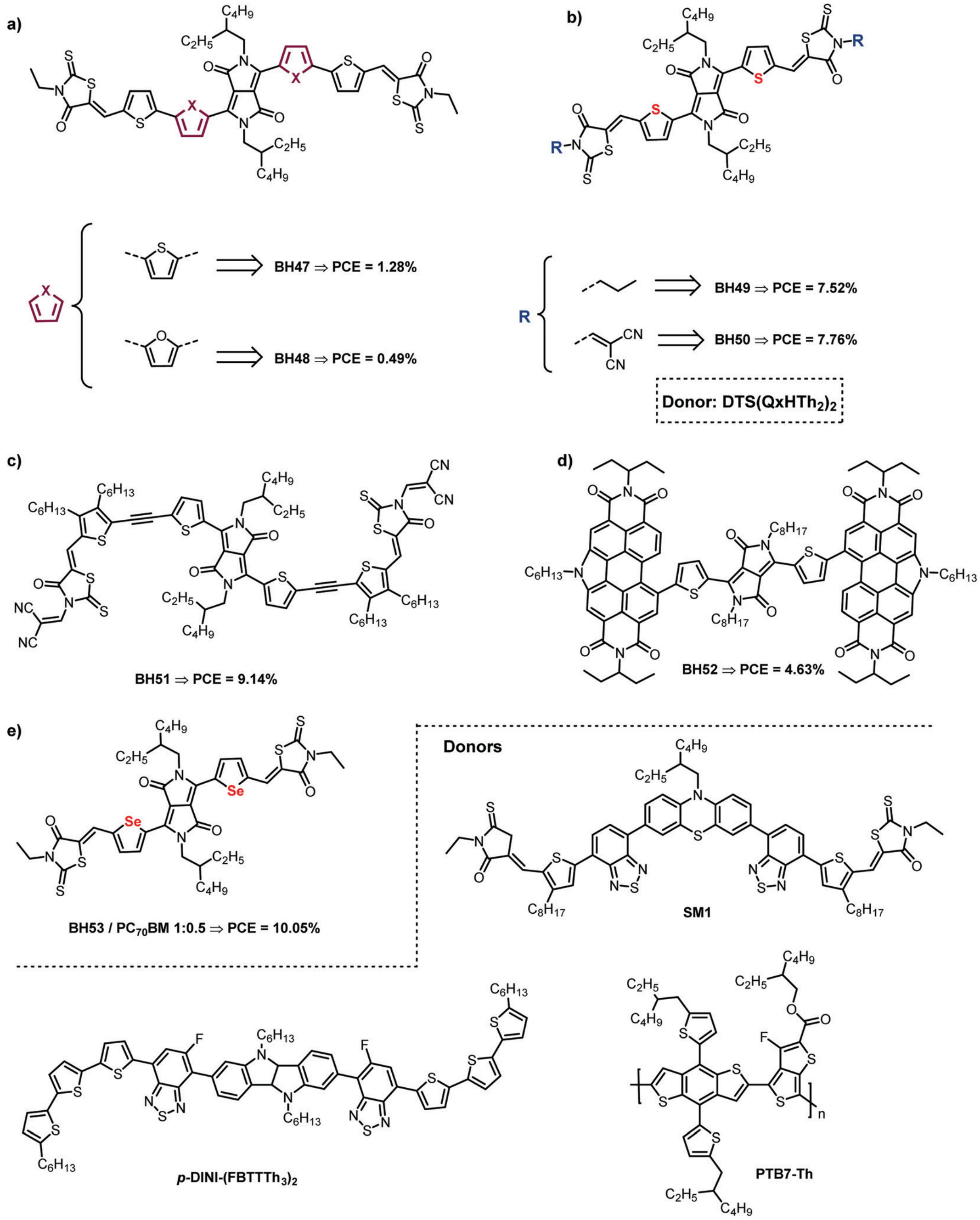

Fig. 11 Chemical structures and the best PCEs for the acceptors **BH47–BH53** and the donors SM1, p-DINI-(FBTTTh$_3$)$_2$.

PCE of 4.47%), but the utility thereof was limited by instability because the alkoxy side chains on the polymer backbone undergo C–O bond cleavage under irradiation.[99,100]

Very recently, Langa *et al.* compared the acceptor **BH49** with its analog with selenophenes (**BH53**, Fig. 11e and Table 4) instead of thiophenes in the structure. When applied in binary mixtures together with the donor SM1 (Fig. 11) in the standard architecture ITO/PEDOT:PSS/active layer/PFN/Al, **BH53** resulted in higher PV parameters, with PCEs of 7.22% and 8.96% for **BH47** and **BH51**, respectively, after SVA. The application of **BH53** in a ternary system, in which PC$_{70}$BM is the co-acceptor and SM1 is the donor, resulted in a remarkable PCE of 10.05%, mainly due to the enhancement in J_{sc} and FF (Table 4).[101]

2.2.2.2. Linear acceptor molecules with a core flanked by DPPs. These molecules are typically of the A–D–A type, in which DPP is the A moiety.

As mentioned in the donors section, Shi *et al.* developed devices with **BH6** as the donor and the acceptor (Fig. 5a). When using **BH6** as acceptor the architecture was ITO/PEDOT:PSS/P3HT (donor):**BH6** (acceptor)/PFN/Al, with D/A ration of 1 : 1. This device exhibited the highest PCE of 3.17% after thermal annealing. Similar PCEs were obtained when **BH6** was used as acceptor or donor. However, although J_{sc} for the **BH6**:$PC_{70}BM$ mixture (8.08 mA cm^{-2}) was higher than that for the P3HT:**BH6** blend (5.35 mA cm^{-2}), V_{oc} for the **BH6**:$PC_{70}BM$ blend is significantly higher than that for the P3HT:**BH6** active layer (1180 *vs.* 890 mV). Thus, due to its twisted molecular conformation, **BH6** exhibited similar HOMO and LUMO energy levels to $PC_{70}BM$ and P3HT, thus providing a good example of the versatility of DPP-based materials.[63]

More interesting studies were carried out using fluorene as the core. Thus, Li *et al.* developed the compound **BH54** (Fig. 12a), which contains a DPP end-capped with thiophene-2-carbonitrile. Given the electronegativity of this group and the conjugation with DPP, **BH54** exhibited a LUMO of −3.65 eV and a narrow bandgap of 1.66 eV. The devices were fabricated using the polymer P3HT as donor material with the standard architecture ITO/PEDOT:PSS/P3HT:**BH54**/PFN/Al and yielded a PCE of 2.37% when DIO was added and after thermal annealing.[102] This same research group replaced the fluorene moiety with a carbazole to give the compound **BH55** (Fig. 12 and Table 4), which exhibited a lower PCE of 2.30%.[103]

Jung *et al.* presented two narrow-bandgap acceptors (**BH56** and **BH57**), whose structure includes a 4,7-dithien-2-yl-2,1,3-benzothiadiazole (DTBT) central core end-capped by two DPP units (Fig. 12b). **BH57** has fluorine atoms in the DTBT core, whereas **BH56** does not The objective of the study was to determine the influence of fluorine on PV performance, for which devices with the inverted architecture ITO/ZnO/PTB7(Fig. 12):Acceptor/MoO_3/Ag were manufactured. The best outcomes obtained using dichlorobenzene as solvent and CN as solvent additive were 3.03% (J_{sc} = 7.77 mA cm^{-2}, V_{oc} = 830 mV and FF = 30%) and 5.00% (J_{sc} = 12.10 mA cm^{-2}, V_{oc} = 810 V and FF = 51%) for **BH56** and **BH57**, respectively. Although the V_{oc} for **BH56** was higher than that for **BH57**, the photo-response of **BH57** was higher, which led to a higher J_{sc} and a 70% higher FF (Table 4).[104]

2.2.2.3. Star-shaped DPP-based acceptor molecules. Another approach has been the synthesis of star-shaped structures in order to imitate the spherical shape of the fullerene π-system,[105–111] which is assumed to be capable of aligning with the donor π-plane in a three-dimensional way, thereby possibly decreasing the Coulomb barrier for charge separation due to enhanced entropic effects and enabling isotropic charge transport.[112,113]

In the study by Gupta *et al.*, a tetraDPP bifluorenylidene H-shaped acceptor was designed and synthesized (**BH58**, Fig. 13a). **BH58** exhibited good solubility and high electron mobility and thermal stability, giving a remarkable PCE of 5.42%.[114] In 2016, Rananaware *et al.* reported a star-shaped acceptor based on tetraphenylethylene functionalized with four DPPs (**BH59**, Fig. 13b). The **BH59** film revealed a strong absorption in the range between 540–800 nm, which matched well with the absorption of the donor P3HT (380–640 nm). The architecture of the device was ITO/PEDOT:PSS/P3HT:**BH59**, using DIO as solvent additive. After thermal treatment this system gave a PCE of 3.86% with one of the highest V_{oc} values for single-molecule BHJ devices based on P3HT as donor to date (V_{oc} = 1.18 V).[115] Liu *et al.* reported a compound with the same backbone as **BH59** with additional phenyl capping on the end of the DPPs (**BH60**, Fig. 13c). In addition, they also synthesized a compound with biphenyl as backbone (**BH61**, Fig. 13e and Table 5) in order to compare both cores. In both cases, the hole and electron mobility and PCE increased after a thermal annealing treatment. The best PCE for P3HT:**BH60** was 2.49%, with a high V_{oc} of 1.16 V, whereas the PCE for P3HT:**BH61** was 1.18% (Table 5).[116] The tetraphenylethylene-DPP was also used as core in the compound **BH62** (Fig. 13d) reported by Sun *et al.*, in which the dicyanovinyl (DCV) electron-withdrawing unit was introduced as end-group. This alteration led to lower frontier energy levels in **BH62** compared to **BH59** and **BH60**. In the same report, the authors also described the PV performance of the compound **BH63** (Fig. 13f and Table 5), the core of which comprises spirobicyclopentadithiophene

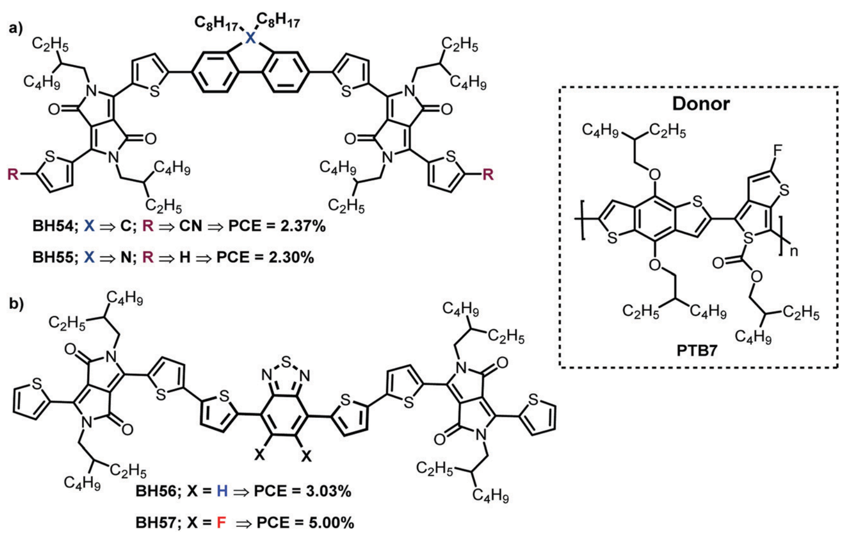

Fig. 12 Chemical structures and PCEs for the acceptors **BH54–BH57** and the donor polymer PTB7.

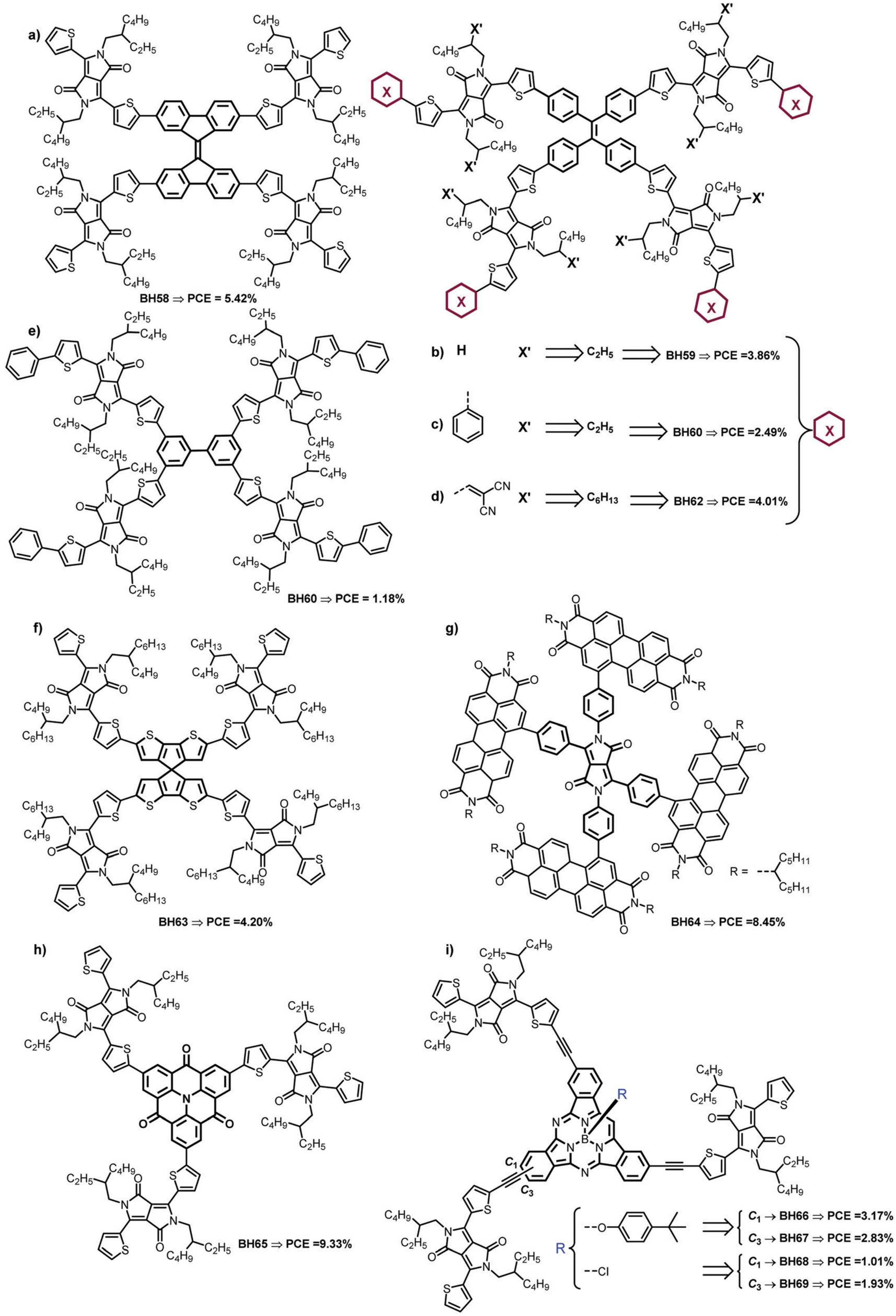

Fig. 13 Chemical structures and PCEs for the star-shaped acceptors **BH58–BH69**.

linked to four DPPs with DCV end-groups. In this case the polymer PTB7-Th was the donor. PTB7-Th:**BH62** exhibited a PCE of 4.01% and PTB7-Th:**BH63** 4.20% (Table 5). **BH63** presented a higher PCE due to the broader UV-vis absorption profile and enhanced charge transport as a result of better conjugation along the arms, exhibiting a higher J_{sc}

Table 5 Donor, LUMO, band gap, additive, architecture, and PV parameters for star-shaped and spirofluorene-DPP-based acceptor single molecules

Acceptor	Donor	LUMO (eV)	Band gap (eV)	Additive[a]	Architecture	J_{sc} (mA cm^{-2})	V_{oc} (mV)	FF (%)	PCE (%)	Ref.
BH58	P3HT	−3.84	1.67	—	Standard	7.74	1170	60	5.42	114
BH59	P3HT	−3.81	1.72	DIO + TA	Standard	3.15	1170	62	3.86	115
BH60	P3HT	−3.64	1.59	TA	Standard	4.45	1160	47	2.49	116
BH61	P3HT	−3.61	1.60	TA	Standard	2.93	1110	36	1.18	116
BH62	PTB7-Th	−3.81	1.59		Standard	9.89	753	54	4.01	117
BH63	PTB7-Th	−3.89	1.42		Standard	11.69	697	47	4.20	117
BH64	PTB7-Th	−3.90	2.09	DIO	Inverted	15.26	850	65	8.45	118
BH65	PTB7	−3.74	1.82	TA	Standard	15.20	1020	61	9.33	119
BH66	PBDB-T	−3.79	1.95	DIO + TA	Inverted	6.42	1170	42	3.17	120
BH67	PBDB-T	−3.74	1.95	DIO + TA	Inverted	5.95	1150	41	2.83	120
BH68	PBDB-T	−3.37	2.04	DIO + TA	Inverted	3.04	930	36	1.01	120
BH69	PBDB-T	−3.40	1.96	DIO + TA	Inverted	4.50	1020	42	1.93	120
BH70	P3HT	−3.60	1.66	TA	Standard	6.96	1100	48	3.63	121
BH71	P3HT	−3.55	1.69	TA	Standard	5.52	880	41	1.87	121
BH72	P3HT	−3.57	1.66	TA	Standard	3.88	910	40	1.42	121
BH73	P3HT	−3.58	1.72	TA	Standard	2.37	750	43	0.76	121
BH74	P3HT	−3.56	1.73	TA	Standard	1.21	790	29	0.28	121
BH75	P3HT	−3.57	1.72	TA	Standard	1.96	700	33	0.45	121
BH76	P3HT	−3.51	1.75	TA	Standard	8.26	1140	55	5.16	122
				—	Inverted	10.23	1110	54	6.09	123
BH77	P3HT	−3.54	1.83	TA	Standard	4.82	930	37	1.67	124
BH78	P3HT	−3.58	1.80	TA	Standard	1.10	810	37	0.33	124
BH79	P3HT	−3.63	1.80	TA	Standard	1.98	1000	37	0.73	124
BH80	PTB7-Th	−3.86	1.56	—	Standard	10.71	740	49	3.85	125
BH81	PTB7-Th	−3.85	1.55	—	Standard	3.22	740	41	0.98	125
BH82	PTB7-Th	−3.89	1.59	—	Standard	1.09	740	32	0.26	125

No additives were used. TA – thermal annealing.

(11.69 mA cm^{-2}) than **BH61** (9.89 mA cm^{-2}) since it contributed more to the photocurrent (Table 5).[117]

A further interesting work is a publication in Chinese in which Hu *et al.* present three PDI-based acceptors that use phenylDPP cores to reduce the planarity of derivatives. All these systems produce amorphous films, which is thought to favor a suitable blend morphology. The four-armed derivative **BH64** displayed the best performance when blended with PTB7-Th (Fig. 13g), with a maximum PCE of 8.45%, a J_{sc} of 15.26 mA cm^{-2}, a V_{oc} of 850 mV and an FF of 65.2% (Table 5) in the inverted architecture ITO/ZnO/Active layer/MoO_3/Al. The authors attributed these results to the fact that the structure with the more expanded conjugation leads to a greater molar extinction coefficient and greater electron transport mobility.[118]

Very recently, Jadhav *et al.* presented a new 3D derivative (**BH65**) that combines a carbonyl-bridged triarylamine core with three DPP blades (Fig. 13h). This compound was applied as NFA together with the donor polymers PTB7 and P3HT in OSCs with the standard architecture ITO/PEDOT:PSS/active layer/Ca/Al. After testing various different manufacturing conditions, it was found that the best performance was obtained with PTB7 after a thermal annealing treatment (110 °C for 5 minutes). The maximum PCE achieved was 9.33%, with a J_{sc} of 15.20 mA cm^{-2}, a V_{oc} of 1020 mV and an FF of 61%, compared with a maximum PCE of 5.62% when the donor was P3HT (J_{sc} = 10.20 mA cm^{-2}, V_{oc} = 910 mV and FF = 60%; see Table 5).[119] In another very recent study reported by Sastre-Santos, Torres and Marsall *et al.*, the synthesis of four DPP-based star-shaped single molecules having subphthalocyanine (SubPc) as central kernel bearing three DPP wings linked by an acetylene bridge (**BH66**, **BH67**, **BH68** and **BH69**, Fig. 13i) were studied. These acceptors featured two different axial groups (4-*tert*-butylphenoxy or chlorine) combined with two possible regioisomers (C_1 and C_3). The aim of this work was to elucidate how the structural variations between the different derivatives affect their optoelectronic properties and consequently the performance of the devices. The four derivatives were applied as NFA materials together with the PBDB-T donor polymer in inverted devices with the architecture ITO/TiO_2/PBDB-T:acceptor/V_2O_5/Ag. After DIO addition and subsequent thermal annealing, **BH66** gave the best performance (PCE = 3.17%), exhibiting a remarkable V_{oc} of 1170 mV (J_{sc} = 6.42 mA cm^{-2} and FF = 42%).[120] For this reason, SubPc-DDP derivatives are high promising NFAs for application in ternary OSCs in which a high V_{oc} is desired.

2.2.2.4. Spirofluorene-DPP-based acceptor molecules. Spirofluorene (SF) is a basic moiety that provides non-planarity to the structures in which it is included, thereby preventing intermolecular aggregation. As some of the molecules mentioned in this section are star-shaped-DPP or linear acceptors, given the number of relevant studies found for this fashionable scaffold, we have decided to give them a subsection.

In 2015, Wu *et al.* developed a series of X-shaped geometries using SF as core with thiophene-DPPs linked by a single bond (**BH70–BH72**, Fig. 14a) and *via* acetylenes (**BH71–BH73**, Fig. 14b).[121] The branched 2-ethylhexyl (EH), linear *n*-octyl (C8) and *n*-dodecyl (C12) alkyl chains were selected as substituents to functionalize the *N*,*N*-positions of the DPP moieties. When blended with P3HT, **BH70** gave a PCE of 3.63%, which is higher than for the equivalent derivatives (PCEs of 1.87% and

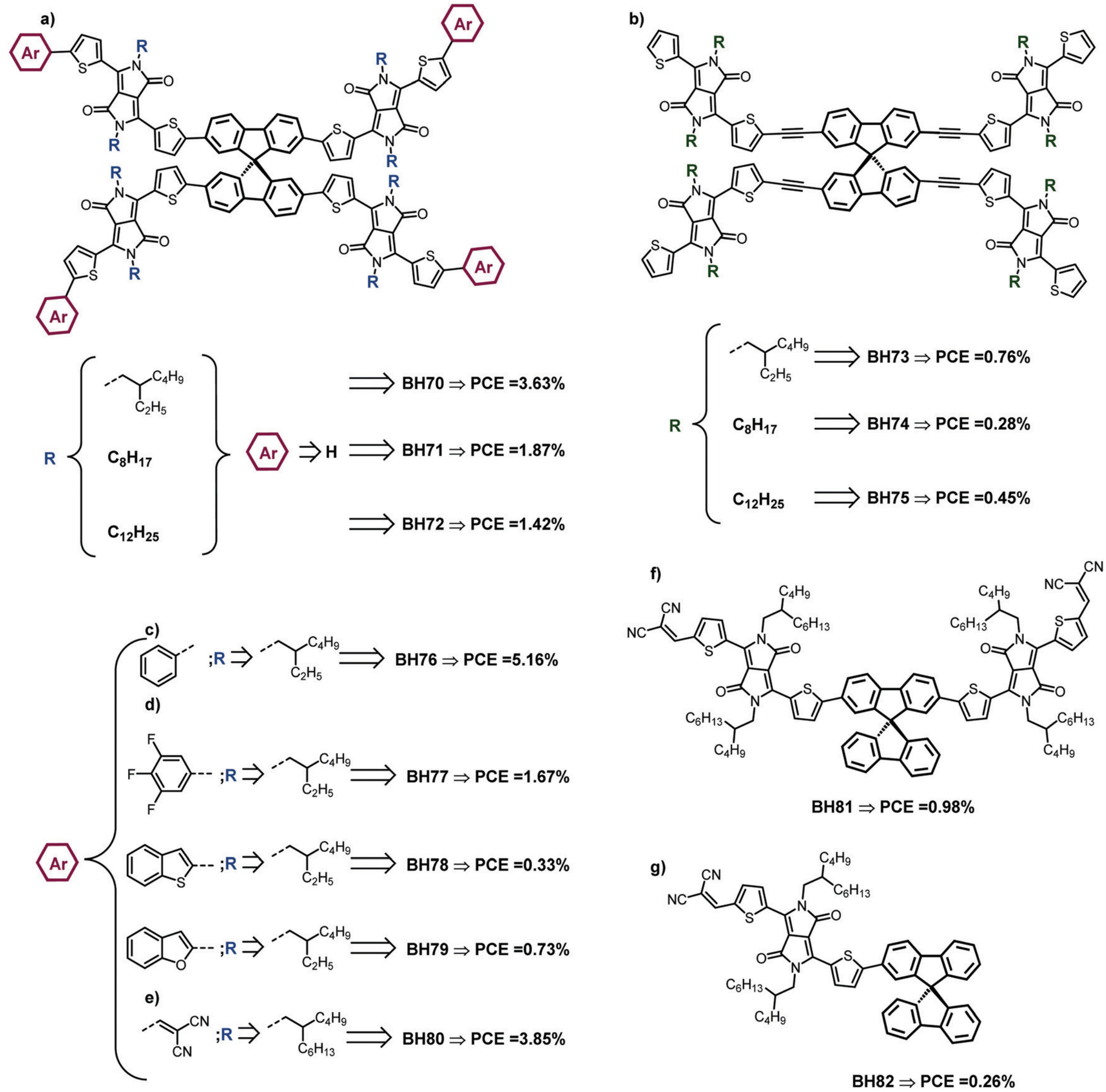

Fig. 14 Chemical structures and PCEs for the spirofluorene-based acceptors **BH70–BH82**.

1.42% for **BH71** and **BH72**, respectively). These results can be explained by the lower crystallinity of **BH71** and **BH72**. The values obtained for the compound with the acetylene bridge were lower, with PCE values of 0.76%, 0.28% and 0.45% for **BH73**, **BH74** and **BH75**, respectively. This was attributed to the fact that the sp^3-hybridized C-bridge blocks electron transfer from the SF core to the DPP units.

In turn, a SF core with four benzene end-capped DPP arms was developed in the study by Li *et al.* (**BH76**, Fig. 14c).[122] Introduction of the benzene rings at the end positions of the DPP led to an improvement in comparison with the analog **BH70** (PCE increased from 3.63% to 5.16%). Furthermore, this system also gave a high V_{oc} value (1.14 V). P3HT:$PC_{60}BM$ exhibited a lower PCE and V_{oc} (3.18% and 620 mV) than P3HT:**BH76** (5.16% and 1140 mV). Moreover, an enhanced PCE of up to 6.09% was reported for the inverted architecture ITO/ZnO/PFN/active layer/MoO_3/Ag by the same authors.[123]

Chen *et al.* also developed an SF-DPP with extended conjugation containing 1,2,3-trifluorobenzene (**BH77**, Fig. 14d), benzo[*b*]thiophene (**BH78**, Fig. 14d) and benzo[*b*]furan (**BH79**, Fig. 14d). These derivatives exhibited a red-shifted absorption compared with **BH70**. The best PCEs using P3HT as donor were 1.67%, 0.33% and 0.73% for **BH77**, **BH78** and **BH79**, respectively. When fused rings were introduced, the solubility decreased markedly, which could affect the morphology of the active layer.[124] Three single molecules were synthesized by Sun *et al.* based on an SF core with a variable number of thiophene-DPP arms and dicyanocinyl as end-group (**BH80–BH82**, Fig. 14e–g). The PTB7-Th:**BH76** blend presented the highest PCE of 3.85% due to its better phase-separation morphology and multiple electronic transmission properties. The PCE for **BH81** and **BH82** was 0.98% and 0.26%, respectively. The 3D structure of **BH82** formed a 3D charge-transport network, thus resulting in an acceptable electron-transport ability, which further leads to a higher J_{sc} (10.71, 3.22 and

1.09 mA cm^{-2} for **BH80**, **BH81** and **BH82**, respectively; Table 5).[125]

OSC performances with DPP-based acceptors are, in general, lower than with DPP-based donors. Looking only at averages, star-shaped designs are more successful as a result of their higher photovoltaic parameters, probably because they give rise to better morphologies. However, linear designs are very promising since the record for this series belongs to one such compound (**BH53**). Unfortunately, there are very few data for linear molecules with DPP flanking a core. Similarly, the parameters for DPP-based acceptors that include a spirofluorene in their structure are quite low. Although the polymeric nature of the donors is predominant, any general conclusion about whether single molecules are more suitable or not could be erroneous even though the record is held by a single molecule counterpart (SM1).

As can be seen, DPP-based donors and acceptors are not among the best single molecules in the active layer of OSCs. However, in our opinion, this should not discourage researchers in the future as these are really promising photoactive molecules that offer a wide range of designs and enhancements that are yet to be discovered.

3. DPPs as sensitizers in dye-sensitized solar cells

Dye-sensitized solar cells (DSSCs) are a photovoltaic technology that first appeared in 1991 in work by Grätzel and O'Regan.[126] Unlike devices that had previously introduced the concept of sensitizer, this type of device has a rough surface on which a large amount of robust dye is adsorbed. This translates into an extensive surface interaction between the different active components that make up the architecture of the device. These systems include three main components: an organic dye, a nanocrystalline semiconductor and a redox couple as mediator in an electrolyte. As an example, they exhibit the typical architecture of an n-type DSSC device using the I^-/I_3^- redox couple in the electrolyte and TiO_2 as semiconductor (Fig. 15a). Thus, these components can be arranged in different architectures, giving rise to n-type and p-type devices. In n-type DSSCs, the operating principle includes the absorption of radiation by the dye, which moves it into the excited state, from which an electron is injected into the conduction band (CB) of the nanocrystalline semiconductor (usually TiO_2). The dye remains oxidized, subsequently returning to its fundamental state due to the mediator present in the electrolyte. Finally, the anode electrons move through an external circuit to reach the counter electrode, where the mediator regenerates. P-Type DSSCs (Fig. 15b), also known as inverted DSSC, typically offering lower performances as NiO has a lower hole mobility (10^{-8}–0.141 cm^2 V^{-1} s^{-1}) and smaller diffusion length for holes (2–3 μm) compared with TiO_2 in n-type DSSCs.[127] The operating principle of a p-type DSSC includes light absorption by the sensitizer to reach its excited state, which then injects a hole into the valence band (VB) of a semiconductor (typically NiO or CuO), thereby reducing the dye, which is regenerated by subsequent reduction of the electrolyte mediator. The latter is regenerated again thanks to the flow of electrons in the external circuit. In the case of sensitizing dyes, both energy levels and electrical properties are relevant. In general, these types of systems have a donor–π-bridge–acceptor (D–π–A) structure. In this structure, the donor unit absorbs the radiation to generate the charge-separated state, from where the charge is transmitted *via* the π-bridge to the acceptor unit, which is usually anchored to the semiconductor *via* a carboxylic acid, cyanoacrylic acid, *etc.* In the case of p-type devices, the charge flow is the same, although in this case holes are injected into the semiconductor. It is worth mentioning that the use of a co-adsorbent agents together with the dye, the mission of which is to passivate the surface of the semiconductor and to modulate the interactions between the dye molecules, mainly to decrease

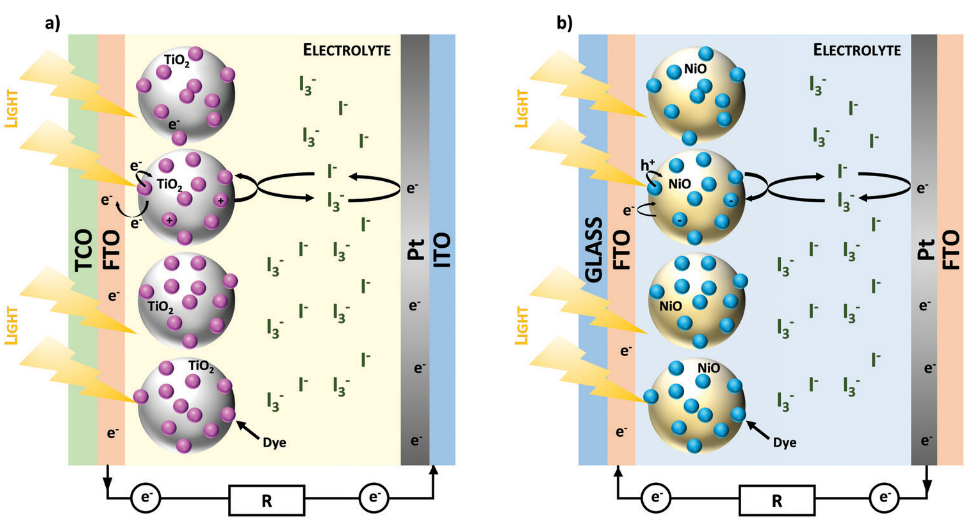

Fig. 15 (a) Scheme of an n-type DSSC device using the I^-/I_3^- redox couple in the electrolyte and TiO_2 as semiconductor, and (b) scheme of a p-type DSSC using the same electrolyte and NiO as semiconductor material.

recombination phenomena, is very common.[128–130] Porphyrin-based dyes have shown the best performance to date, with PCEs of more than 13%.[131–133] Nevertheless, due to their electronic character, DPPs are highly suitable moieties for both n-type and p-type devices, therefore they have been applied quite successfully as dyes in this technology.

The first mention in English in the literature regarding the use of DPPs in DSSCs is a patent from 2009.[134] Articles describing the application of DPPs as sensitizers in DSSCs can be found since 2010.[135,136] In the first published study, two non-linear DPP systems (**D1** and **D2**, Fig. 16 and Table 6), in which the donor units are two different triarylamines, without substituents and with *p*-methoxy groups in the more distal benzene rings, are compared in a n-type device. A PCE of 2.68% was obtained with derivative **D1** without the use of co-adsorbent. In the case of **D2**, a maximum PCE was achieved using chenodeoxycholic acid (CDCA). There has been extensive research into the use of DPPs as sensitizers in DSSCs since then.[137–140] The most prominent examples since 2015 are discussed briefly below.

3.1. DPP-based single molecules as sensitizers in n-type DSSCs

Although we will focus on studies published since 2015, the highest PCE for an n-type DSSC sensitized with DPP derivatives was achieved in 2013 using molecule **D3** in the presence of the co-adsorbent CDCA (Fig. 16b and Table 6). In that article, four asymmetric DPP derivatives that differ only in terms of the donor moiety are compared. These derivatives are studied using both computational calculations and spectroscopically

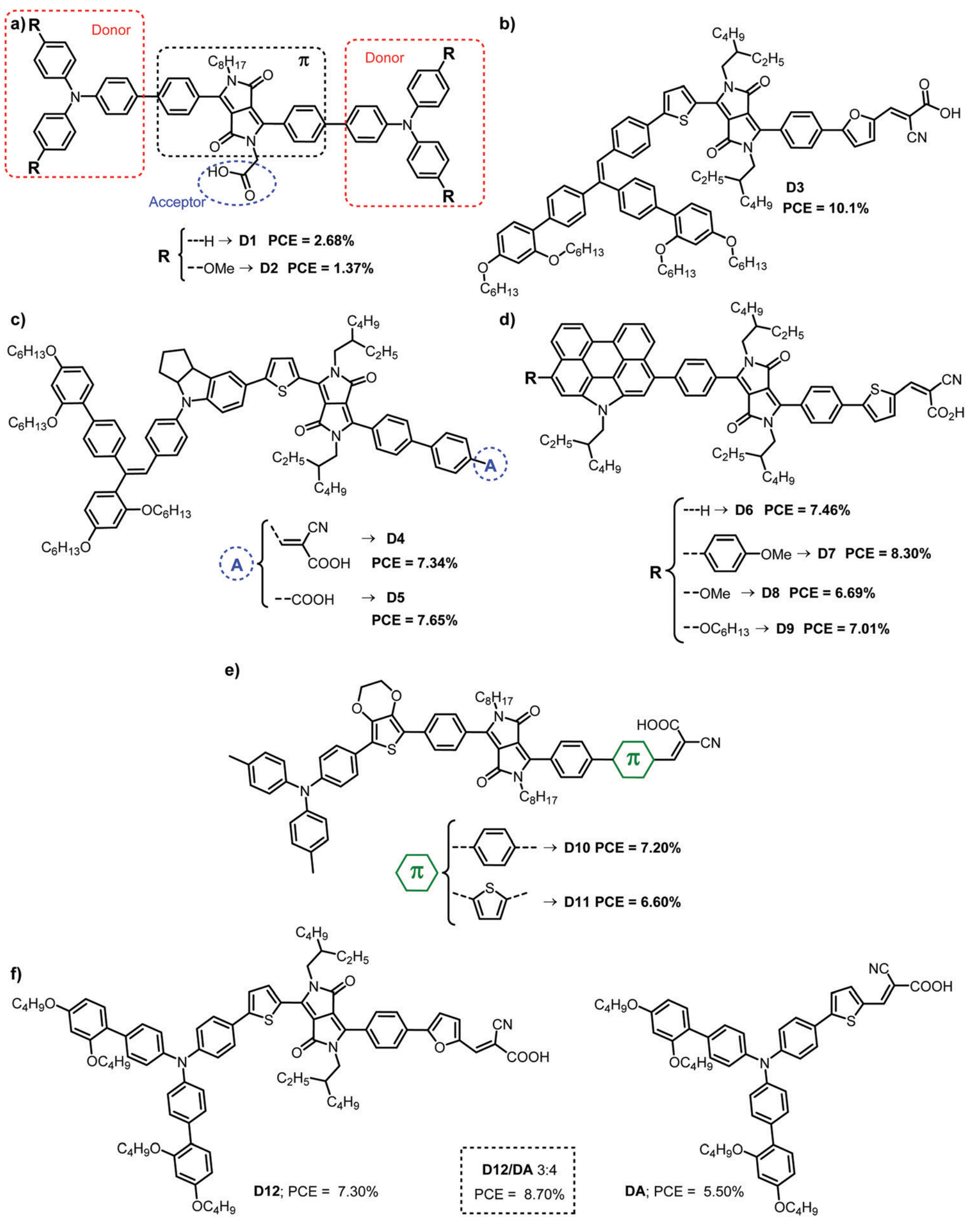

Fig. 16 Chemical structures and PCEs for **D1–D12** and **DA**.

Table 6 Electrolyte, co-adsorbent and photovoltaic parameters for dyes **D1–D30**

Dye	Electrolyte	Co-adsorbent	J_{sc} (mA cm^{-2})	V_{oc} (mV)	FF (%)	PCE (%)	Ref.
D1	I^-/I_3^-	No	9.57	455	58	2.68	135
D2	I^-/I_3^-	CDCA	5.49	423	59	1.37	135
D3	$Co[(bpy)_3]^{3+/2+}$	CDCA	17.90	761	74	10.10	141
D4	I^-/I_3^-	CDCA	15.28	698	69	7.34	142
D5	I^-/I_3^-	CDCA	14.86	687	75	7.65	142
D6	I^-/I_3^-	CDCA	15.29	675	72	7.46	143
D7	I^-/I_3^-	CDCA	17.14	698	69	8.30	143
D8	I^-/I_3^-	CDCA	14.60	639	72	6.69	143
D9	I^-/I_3^-	CDCA	15.59	643	70	7.01	143
D10	I^-/I_3^-	CDCA	12.70	762	74	7.20	144
D11	I^-/I_3^-	CDCA	12.30	711	76	6.60	144
D12	$[Co^{3+}]/[Co^{2+}]$	—	15.60	797	70	8.70	145
D13	I^-/I_3^-, *t*BP	DCA	19.40	480	53	4.90	147
D14	I^-/I_3^-, *t*BP	DCA	13.60	680	66	6.10	147
D15	I^-/I_3^-	CDCA	14.21	670	64	6.14	150
D16	EMI-TBC/PMII, /*t*BP	—	15.20	678	71	7.1	151
D17	I^-/I_3^-	CDCA	11.01	513	61	3.43	152
D18	I^-/I_3^-	CDCA	11.30	539	59	3.62	152
D19	I^-/I_3^-	CDCA	0.75	125	37	0.03	154
D20	I^-/I_3^-	CDCA	1.51	135	32	0.07	154
D21	$[Co^{3+}]/[Co^{2+}]$	CDCA	1.62	365	31	0.18	154
D22[a]	I^-/I_3^-	—	1.89	100	33	0.063	155
D23[a]	I^-/I_3^-	—	1.44	84	33	0.040	155
D24[a]	$[Co^{3+}]/[Co^{2+}]$	—	2.06	330	30	0.205	155
D25[a]	$[Co^{3+}]/[Co^{2+}]$	—	1.95	370	29	0.210	155
D26[a]	I^-/I_3^-, GuSCN, TBP	—	0.26	74	53	0.008	156
D27[a]	I^-/I_3^-, GuSCN, TBP	—	0.70	81	25	0.010	156
D28[a]	I^-/I_3^-, GuSCN, TBP	—	7.38	147	32	0.35	156
D29[a]	I^-/I_3^-, GuSCN, TBP	—	4.04	123	32	0.16	156
D30	$PC_{60}BM$	CDCA	0.32	228	32	0.023	157

[a] Average values are provided.

and photovoltaically. A PCE of 10.10% was achieved with **D3** when combined with the electrolyte $Co[(bpy)_3]^{3+/2+}$.[141] In 2015, Ganesan *et al.* compared two DPP-based dyes to determine the influence of the different strength of the acceptor unit on light harvesting and the electrochemical and photovoltaic properties of DSSC devices containing CDCA. Here, the strong acceptor cyanoacrylic acid (**D4**) is compared with the weaker acceptor carboxylic acid **D5** (Fig. 16c and Table 6). The difference in optoelectrochemical properties was found to be not significant. However, a better photovoltaic result was obtained with **D5**, with a J_{sc} of 14.86 mA cm^{-2}, a V_{oc} of 687 mV, an FF of 75% and a PCE of 7.65% under simulated one sun *versus* a PCE of 7.34% with the cyanoacrylic acid group.[142] The same year, Li *et al.* published a paper in which they described four molecules with a D–π–A–π–A structure, with *N*-annulated perylenes as the donor groups (**D6–D9**, Fig. 16d and Table 6). These authors studied the effect of additional electron-donating substituents at a *peri* position of the perylene and found that the bulky 4-methoxyphenyl group attached at this *peri* position can reduce charge recombination and enhance V_{oc}, thus making derivative **D7** the most efficient of the four with and without CDCA. Therefore, **D7** with co-adsorbent showed a PCE of 8.30% with a J_{SC} of 17.14 mA cm^{-2}, a V_{oc} of 698 mV and an FF of 69%.[143] Similarly, Chiu *et al.* synthesized and studied two DPP-based dyes (**D10** and **D11**, Fig. 16e and Table 6) with 4,4′-ditolylaniline as the donor and cyanoacrylic acid as the acceptor and anchoring group. The objective was to elucidate how the presence of phenyl (**D10**) or thienyl (**D11**) spacers influences the photovoltaic properties of the devices fabricated in the presence of CDCA. Although **D11** had a very high molar extinction coefficient at 530 nm (2.25×10^5 M^{-1} cm^{-1}) and a lower bandgap, **D10** demonstrated better performance (PCE = 7.20% *vs.* 6.60% for **D11**) due to its better ability to inject electrons into TiO_2 as a result of its linear structure, as shown by density functional theory (DFT) calculations and femtosecond time-resolved photoluminescence data.[144]

A further interesting study was published by Hao *et al.*, in which these authors described how the correct co-sensitization between red and blue D–π–A organic dyes leads to an improvement in the performance of solar cells. Thus, the blue DPP **D12** was combined with the red dye **DA** in a 3 : 4 ratio, which resulted in an increase in PCE from 7.30% and 5.50%, respectively, separately to a PCE of 8.70% when combined, using the cobalt-based electrolyte tris(2,2′-bipyridyl)cobalt(II/III) ($[Co(bpy)_3]^{3+/2+}$) under AM 1.5G (Fig. 16f and Table 6).[145]

Shimogawa *et al.* designed and synthesized two low-bandgap DPP-based sensitizers that included boryl-substituted thienylthiazole moieties in the acceptor group (**D13** and **D14**). **D13** and **D14** possess octyl and 2,6-dialkoxybenzyl groups on the lactam nitrogen atoms of the DPP unit, respectively (Fig. 17a and Table 6). The DPP group was introduced into the system as an enhancement to a previous prototype,[146] namely the **DB** sensitizer. As a result of this modification, the two DPP-based derivatives have more suitable HOMO and LUMO levels with a narrower bandgap than **DB**. The best performance was obtained with **D14** (J_{sc} = 13.60 mA cm^{-2}, V_{oc} = 680 mV, FF = 66%, and

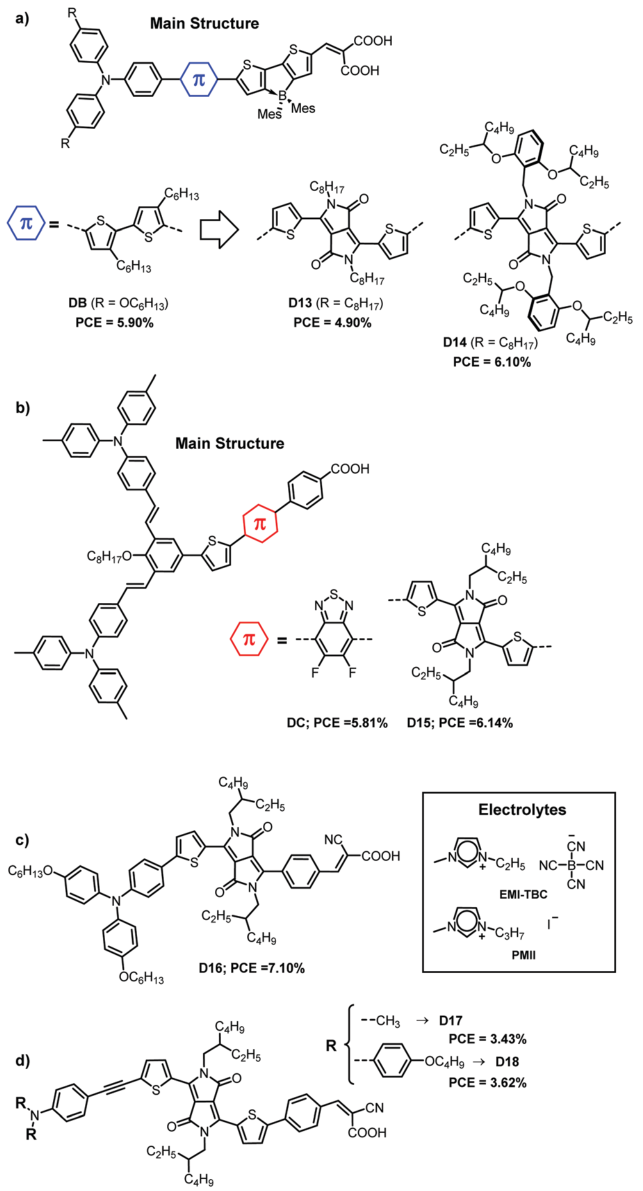

Fig. 17 Chemical structures and PCEs for **D13–D18**.

PCE = 6.10%), with deoxycholic acid (DCA) as co-adsorbent and 4-*tert*-butylpyridine (*t*BP) as additive.[147] TBP in I^-/I_3^- electrolyte solution increases the CB edge potential of TiO_2, thus leading to an increase in V_{oc} and a decrease in electronic recombination by preventing the access of I_3^- to the TiO_2 surface.[148,149] Similarly, Wang *et al.* reported the synthesis of two D–π–A–π–A systems (**DC** and **D15**, Fig. 17b and Table 6) with *N*,*N*-di-*p*-tolylanilinyl in the donor moiety. These authors studied the impact of the difluorobenzo[*c*][1,2,5]thiadiazole or DPP auxiliary acceptor on the photophysical and electrochemical properties and DSSC performance. The DPP-containing molecule **D15** exhibited a higher J_{sc} due to its high molar extinction coefficient at higher wavelengths and its wider absorption spectrum, which ranges from the visible to the near-infrared region, thus generating a greater photocurrent than its counterpart. A longer electron lifetime and increased charge recombination resistance were observed for **DC**, thus resulting in a higher V_{oc}. DSSC devices sensitized with **D15** showed better performance (J_{sc} = 14.21 mA cm^{-2}, V_{oc} = 670 mV, FF = 64%, and PCE = 6.14%) than those containing **DC** (J_{sc} = 11.01 mA cm^{-2}, V_{oc} = 750 mV, FF = 71%, and PCE = 5.81%) when CDCA was used a co-adsorbent.[150] Decoppet *et al.* developed different binary ionic liquid electrolytes based on 1-methyl-3-propylimidazolium iodide salts and also investigated the influence of adding lithium ions to the electrolyte to enhance the DSSC device performance, together with the DPP-based sensitizer **D16** (Fig. 17c and Table 6). The best device exhibited a short-circuit current density of 15.20 mA cm^{-2}, a V_{oc} of 678 mV and an FF of 71%, corresponding to an overall PCE of 7.1%, under standard AM 1.5G illumination at 100 mW cm^{-2} with the electrolyte mixture EMI-TBC/PMII 1 : 1 in the presence of I_2 and *N*-butylbenzimidazole.[151]

In a recent study by Lim *et al.*, the synthesis of blue-colored dyes featuring a DPP spacer with dimethylamine and bis(4-dibutoxylphenyl)phenylamine as donor residues (**D17** and **D18**, Fig. 17d and Table 6) was reported, together with their spectroscopic, electrochemical and colorific properties and their application in translucent DSSCs. In the DSSCs fabricated with 5 μm-thick TiO_2 photoanodes and CDCA as co-adsorbent, **D17** and **D18** yielded PCEs of 3.43% and 3.62%, respectively, under simulated one sun illumination.[152]

3.2. DPP-based single molecules as sensitizers in p-type DSSCs

As mentioned at the beginning of this section, DSSC p-type devices are generally less efficient than n-type devices since they still face many challenges. The current record was published by Perera *et al.* in 2015, with a PCE of 2.51% and an amazing J_{sc} of 7.65 mA cm^{-2}.[153] These authors used an electrolyte based on the tris(acetylacetonato)iron(III)/(II) redox couple ($[Fe(acac)_3]^{0/1-}$) and a perylene-thiophene-triphenylamine sensitizer (**DD**; Fig. 18a and Table 6). The first study of DPP-based sensitizers was published by Favereau *et al.* in 2013. In this paper, three diphenylDPP systems with thienyl carboxylic acid as the anchoring group and with a bromine (**D19**), a malononitrile (**D20**) or a naphthalenediimide (NDI) (**D21**) as acceptor moiety were compared (Fig. 18b and Table 6). All DPP derivatives were tested with I^-/I_3^- electrolyte, but only **D21** was used with $[Co^{3+}]/[Co^{2+}]$ electrolyte, in this latter case obtaining the best result in the presence of CDCA, with a J_{sc} of 1.62 mA cm^{-2}, a V_{oc} of 365 mV, an FF of 31% and a PCE of 0.18%.[154] These authors also presented other molecules based on diphenylDPPs with a dicarboxylated triphenylamine, an anchoring group for attachment to NiO, and bromine (**D22** and **D23**) or NDI (**D24** and **D25**) as acceptor group. DSSC devices were fabricated with the classic electrolyte I^-/I_3^- and with cobalt(II/III)–polypyridine electrolytes (Fig. 18c and Table 6). Those dyes containing the NDI acceptor unit yielded higher photovoltaic performances, exhibiting larger charge separation state lifetimes than those with bromine. In addition, the devices containing cobalt(II/III)–polypyridine electrolytes showed better results.[155] The same authors subsequently reported a series of four analogues with structural modifications. Thus, they replaced diphenylDPP with dithienylDPP, including the dicarboxylated triphenylamine

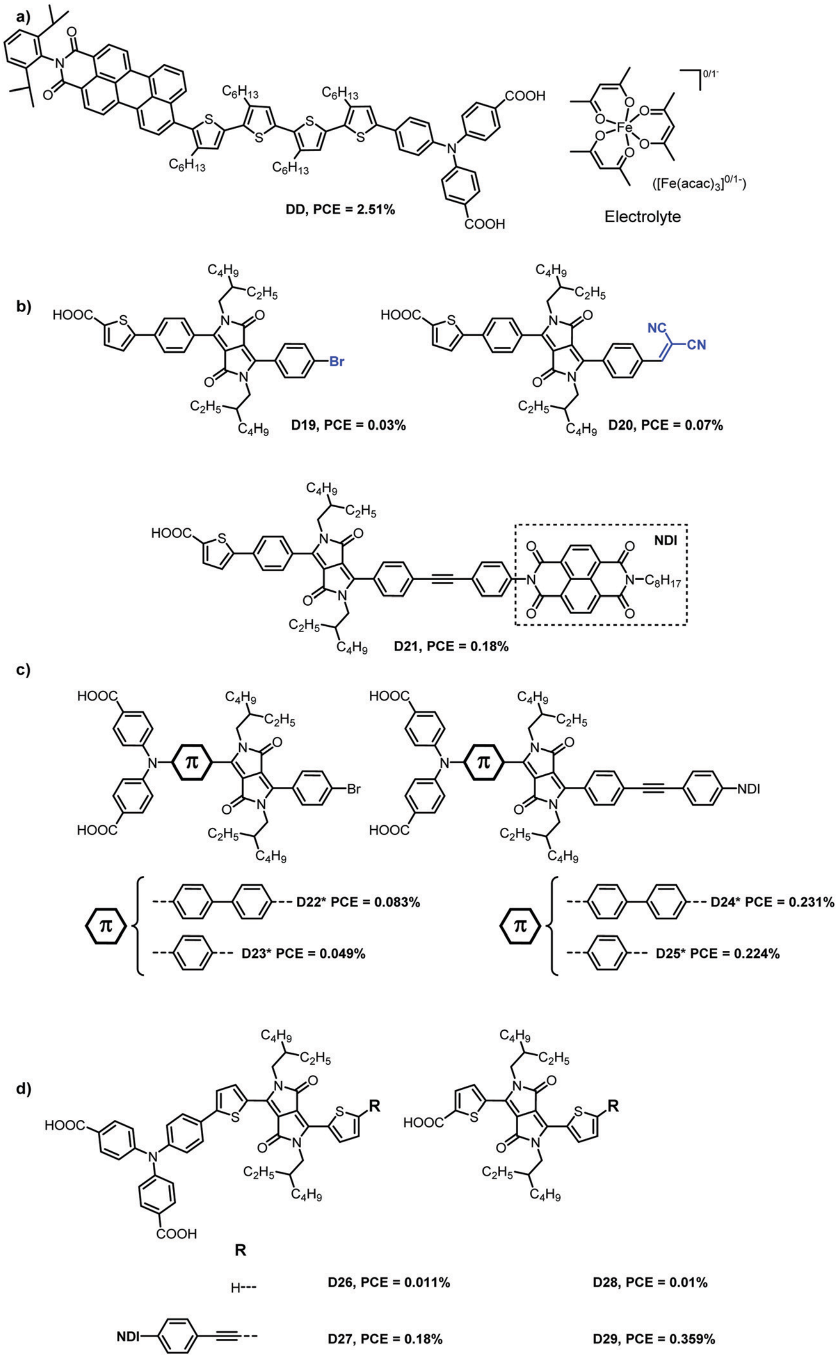

Fig. 18 Chemical structures and PCEs for **D19–D29** sensitizers for p-type DSSCs. *Maximum PCEs are provided.

anchoring group in **D26** and **D27**, but replacing it with a thienyl carboxylic acid in **D28** and **D29**, and including the NDI acceptor group also connected *via* a triple bond in **D27** and **D29** (Fig. 18d and Table 6). As result of these modifications, these derivatives exhibited higher molar extinction coefficients at longer wavelengths than their diphenyl counterparts. More importantly, these modifications led to a notable improvement in performance, achieving a PCE 0.35%, a V_{oc} of 149 mV, an FF of 33% and a J_{sc} of 7.40 mA cm^{-2} with sensitizer **D29**.[156]

DPP-sensitizers for p-type solid-state DSSC have also been reported by Odobel's group in a study published in 2017. Two DPP derivatives with carboxylic acid as the anchoring group were presented. One of them (**D30**, Fig. 19 and Table 6) contains pyromellitimide (PYRO) as the acceptor substituent. This compound plays the role of a secondary inner electron acceptor to inject exited electrons into the known electron-transporting material $PC_{60}BM$ more efficiently by promoting the fast formation of a $DPP^{+}/PCBM^{-}$ charge-separated state. A J_{sc} value of up to 0.45 mA cm^{-2} was achieved with the previously mentioned **D23**, which is 10 times larger than previously reported values for this kind of device.[157,158]

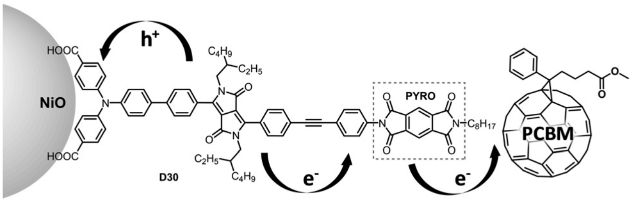

Fig. 19 Chemical structure of **D30** for p-type solid-state DSSCs. Adapted from Pham *et al.*[157]

In summary, with regard to DPP-based sensitizers, there is still a long path to walk in view of the state of the art, although these systems clearly have a potential that is yet to be exploited. It is likely that their tendency to aggregate limits their utility in DSSCs, and recombination phenomena may occur with high probability.

In light of the state of the art, n-type devices are superior to their p-type counterparts in this series. The highest PCE for an n-type device is currently 10.1% for **D3** when the redox pair $Co[(bpy)_3]^{3+/2+}$ was applied as electrolyte and CDCA was the co-adsorbent. As such, given that DPPs are not far from the current record (≈13%), perseverance in design may lead to outstanding performance in the futures.

4. DPP-based single molecules in perovskite solar cells

Perovskite solar cells (PSCs) represent a revolution in the field of photovoltaics. This technology has achieved great attention due to the high efficiencies being achieved, which can even exceed 25%.[159,160] Although progress is being made in this regard, long-term stability remains a challenge preventing their entry into the market.[161–163] Perovskites are crystalline structures of the ABX_3 type in which A is typically an organic cation, such as methylammonium (MA) and/or formamidinium (FA), or an inorganic cation such as cesium or rubidium, B is a metal, generally lead, or, to a lesser extent, tin, and X is a halogen (iodine, bromine or chlorine) (Fig. 20a). The configuration of PSCs can differ depending on the architecture used, and can be mesoporous n–i–p (Fig. 20b), planar n–i–p (Fig. 20c) and planar p–i–n (Fig. 20d). The layers that make up these devices are typically a glass on which the contact is deposited (electron-selective for n–i–p configuration and hole-selective for p–i–n configuration), followed by an electron- or hole-transporting layer (ETL or HTL), then the active or perovskite layer is added (planar or mesoporous). This layer is then covered with another hole- or electron-transporting layer, and finally by a metal contact for the charges to flow. The outermost layer immediately below the metal electrode (ETL or HTL) must let some charges pass and block others (*e.g.*, the ETL must let electrons pass and prevent the passage of holes to minimize recombination phenomena) and should also protect the device against damage, such as by moisture. The single molecule 2,2′,7,-7′-tetrakis(*N*,*N*-di-*p*-methoxyphenylamine)-9,9′-spirobifluorene (spiro-OMeTAD, Fig. 21a) and the polymer poly(triarylamine) (PTAA) are commonly used HTMs to fabricate n–i–p PSCs, and PCBM is a common ETL in p–i–n devices. It is necessary to add doping agents to these materials in small proportions to obtain high

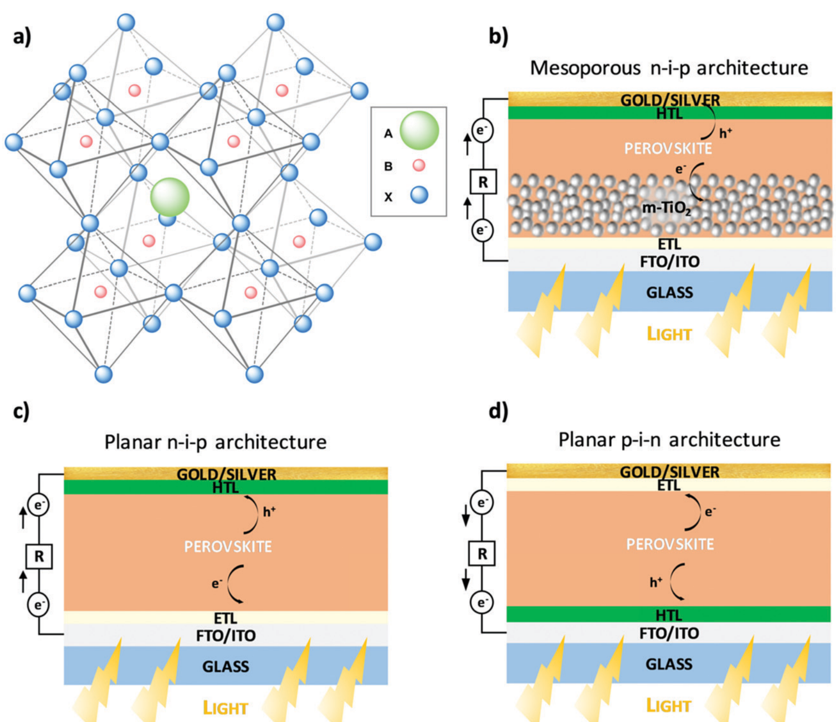

Fig. 20 (a) Representation of the PSC crystalline structure (*e.g.*, A = FA, MA, Cs, Rb; B = Pb, Sn; X = I, Br, Cl), (b) a mesoporous n–i–p architecture device, (c) a planar n–i–p architecture device, and (d) a planar p–i–n device.

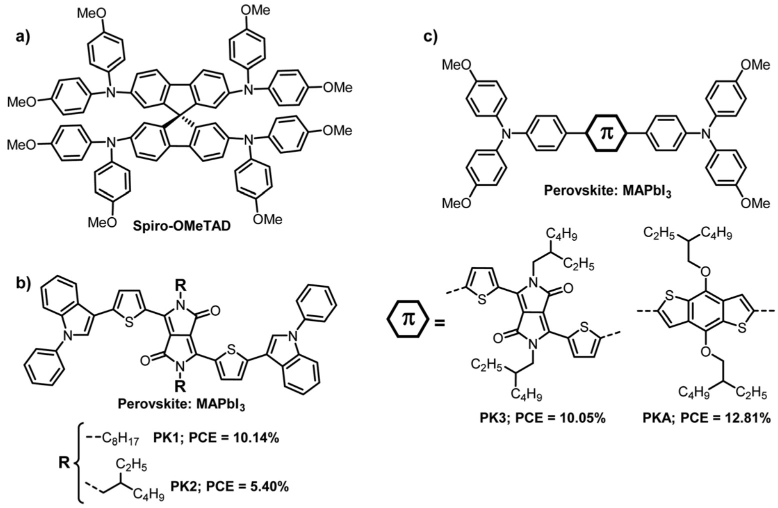

Fig. 21 (a) Chemical structure of spiro-OMeTAD, (b) chemical structures and PCEs for **PK1** and **PK2**, (c) chemical structures and PCEs for **PK3** and **PKA**. Perovskite compositions are included.

performance devices, typically *t*BP or the salt lithium bis(trifluoromethanesulfonyl)imide (Li-TFSI). However, these dopants are hygroscopic in nature, therefore their presence affects the stability of the PSCs.[164–166] As such, it is of interest to develop new HTMs that do not need to be doped to ensure a good performance.

DPP-based materials can exhibit high charge carrier mobility in conjugated systems, good crystallinity, tend to be robust and have a great chemical versatility. Due to these remarkable properties, they are good candidates for application as HTMs or ETMs in PSCs.[167,168]

4.1. DPP-based single molecules as hole-transporting materials in PSCs

The use of DPPs in PSCs has not been widely studied to date, although some interesting recent reports can be found. Indeed, studies of DPP-based single molecules as HTMs are the most abundant. The values for the HOMO levels and hole mobilities are crucial parameters since they determine if the HTM will be able to extract holes from the active layer and conduct them to the electrode efficiently. These values, together with the PV parameters for the best devices including DPP-HTMs, are presented in Table 7. In 2016, Jeon *et al.* published an interesting article describing the study of two bis-*N*-phenylindolyl-DPP single molecules as dopant-free HTMs in $MAPbI_3$ PSCs with two different *N*-alkyl chains: one linear (*n*-octyl, **PK1**) and another one branched (2-ethylhexyl, **PK2**) (Fig. 21b). The side chain determines how the molecules arrange in the solid state, thereby affecting the hole extraction ability and charge conductivity of the layer. The linear chain in **PK1** causes the molecules to have a strong tendency to aggregate in the film, whereas **PK2** films have an amorphous nature, as elucidated by two-dimensional grazing-incidence X-ray diffraction. This means that **PK1** exhibits higher molar extinction coefficients

Table 7 Perovskite composition, hole mobility, HOMO values and the best PV parameters for **PK1–PK10** DPP-based HTMs

HTM	Perovskite	μ_h ($cm^2 V^{-1} s^{-1}$)	HOMO (eV)	Dopant	$-J_{sc}$ ($mA cm^{-2}$)	V_{oc} (V)	FF (%)	PCE (%)	Ref.
PK1	$MAPbI_3$	—	−4.90	No	15.1	0.96	70.0	10.14	169
PK2	$MAPbI_3$	—	−4.90	No	15.2	0.86	41.0	5.40	169
PK3	$MAPbI_3$	—	−5.13	Li-TFSI/*t*BP	16.6	0.92	66.0	10.05	170
PK4	$MAPbI_3$	—	−5.20	Li-TFSI/*t*BP	10.0	0.97	53.0	5.10	171
PK5	$MAPbI_3$	—	−5.21	Li-TFSI/*t*BP	14.4	0.97	71.0	9.85	171
PK6	$MAPbI_3$	—	−5.22	Li-TFSI/*t*BP	10.9	1.01	74.0	8.16	171
PK7	$MAPbI_3$	1.38×10^{-4}	−5.15	No	—	—	—	8.63	172
PK8	$MAPbI_3$	9.85×10^{-5}	−5.16	No	—	—	—	8.39	172
PK9	$MAPbI_3$	5.32×10^{-4}	−5.12	Li-TFSI	21.5	0.94	68.4	14.13	172
				No	20.6	0.94	64.8	12.87	
BH34	[a]	—	−4.90	No	20.6	1.10	73.8	16.80	174
PK10	$MAPbI_3$	2.53×10^{-4}	−4.87	No	14.4	0.93	60.2	8.32	175
PK11	$MAPbI_3$	5.89×10^{-4}	−4.84	No	17.7	0.92	63.2	11.16	175
PK12	$MAPbI_3$	6.43×10^{-4}	−4.89	No	19.8	0.94	64.0	12.05	175
PK13	$MAPbI_3$	1.09×10^{-3}	−4.97	No	22.3	1.05	71.1	17.64	
		1.84×10^{-3}		LiTFSI	22.9	1.14	73.9	20.19	

[a] $[Cs_{0.05}(FA_{0.83}MA_{0.17})_{0.95}]Pb(I_{0.83}Br_{0.17})_3$.

at higher wavelengths than **PK2**, as characterized by UV-vis spectroscopy. Devices made with **PK1** performed better than those with **PK2** (PCE of 10.14% *vs.* 5.40%, respectively, measured in a reverse voltage scan). Moreover, an IPCE study showed that **PK1** contributes to light harvesting. In addition, time-resolved photoluminescence and transient photovoltage studies showed that the **PK1**-based device exhibited better charge extraction ability and lower charge recombination than the control dopant-free spiro-MeOTAD-based device.[169] The same year, and also using $MAPbI_3$ as active layer, Liu *et al.* presented a study in which they compared a new DPP-based HTM (**PK3**) with a new benzodithiophene-based single molecule (**PKA**) and spiro-OMeTAD in control PSCs (Fig. 21c). The optimized devices fabricated with doped **PK3** HTM exhibited a J_{sc} of 16.60 mA cm^{-2}, a V_{oc} of 0.92 V, an FF of 66% and a PCE of 10.05%, all of which were lower than in the case of the doped **PKA** (PCE of 12.81%). Both **PK3** and **PKA** demonstrated greater stability than spiro-OMeTAD after aging for 10 days, with a 13% and 14% loss of PCE, respectively, *vs.* a 36% PCE loss in the case of spiro-OMeTAD.[170]

Three DPP-based D–π–A–π–D systems were published in 2018 (**PK4**, **PK5** and **PK6**, Fig. 22a) as part of a study of the effect of two different donor groups (triphenylamine and phenothiazine) and two π-bridges (benzene and thiophene) on PSC performance. **PK5** gave the best photovoltaic performance (J_{sc} = 14.35 mA cm^{-2}, V_{oc} = 0.97 V, FF = 71% and PCE = 9.85%, *vs.* 5.10% and 8.16% for **PK4** and **PK6**, respectively). The structure of **PK5** contains thiophenes as π-bridges and two terminal triphenylamine donor groups. The dihedral angle between the DPP core and the thiophene ring is smaller than that for benzene, which could lead to better organized morphologies and better hole mobilities. The HOMO levels of these three systems are similar, and all of them have adequate LUMO levels to block the flow of electrons. Additionally, a shorter photoluminescence lifetime was

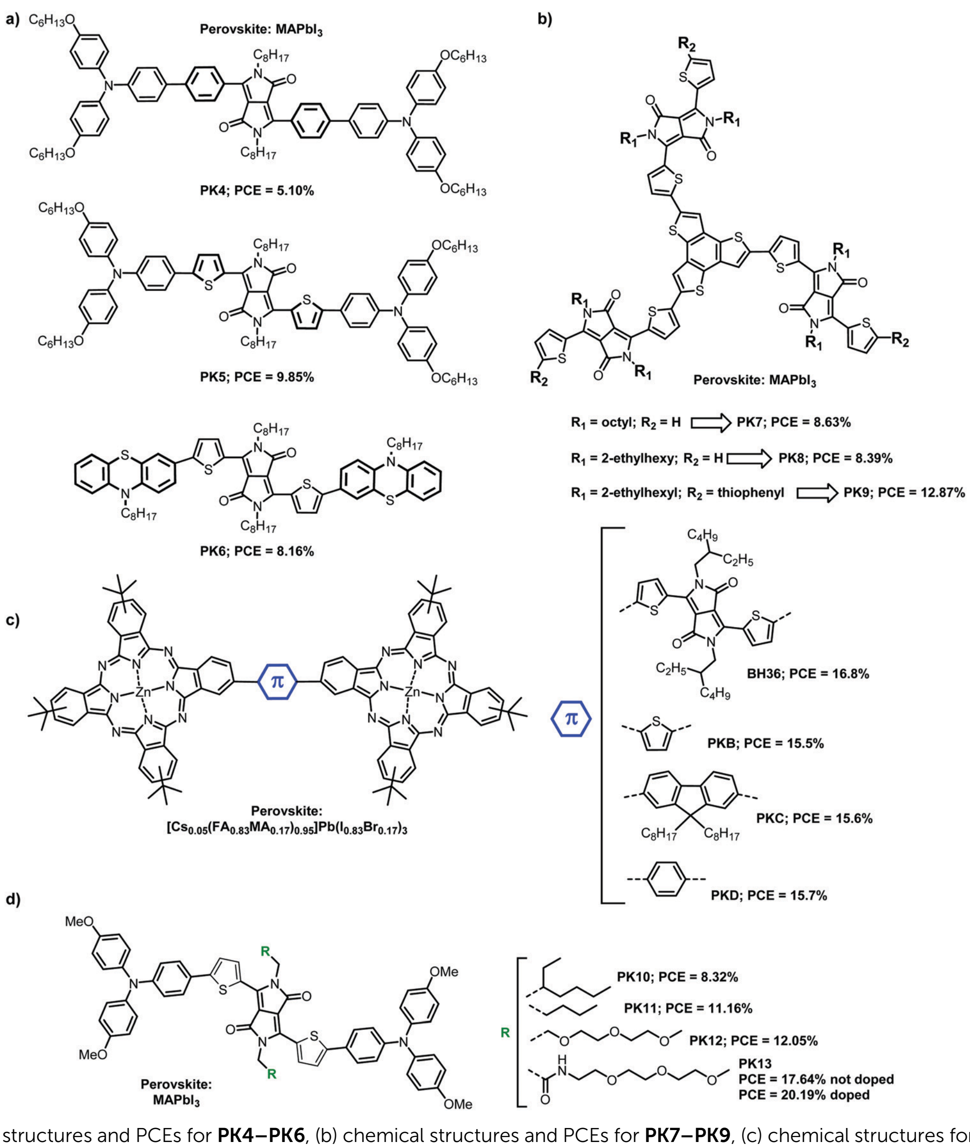

Fig. 22 (a) Chemical structures and PCEs for **PK4–PK6**, (b) chemical structures and PCEs for **PK7–PK9**, (c) chemical structures for **BH36**, **PKB**, **PKC** and **PKD**, (d) chemical structures and PCEs for **PK10–PK13**. Perovskite compositions are included.

observed for **PK5** (1.65 ns) by time-resolved photoluminescence than for **PK4** and **PK6** (9.02 ns and 2.69 ns, respectively), which can be attributed to a better ability to extract holes.[171] Three star-shaped systems based on benzo[1,2-*b*:3,4-*b*′:5,6-*b*″]trithiophene and DPP building blocks were published in 2019 by Kim *et al* (**PK7**, **PK8** and **PK9**; Fig. 22b). Differences in PSC performance upon variation of the DPP side chain and extension of the conjugated structure after adding a terminal thiophene ring were studied. Dopant-free **PK9**, the structure of which comprises a 2-ethylhexyl side chain and an extra terminal thiophene ring, exhibited the best PCE of 12.87%, with corresponding photovoltaic parameters V_{oc} = 0.94 V, J_{sc} = 20.60 mA cm^{-2} and FF = 64.8%. This PCE value is higher than those for the other two HTMs **PK7** and **PK8**, which exhibited PCEs of 8.63% and 8.39%, respectively. A marked improvement was obtained when **PK9** was doped with Li-TFSI, with a PCE of 14.13%, a V_{oc} of 0.94 V, a J_{sc} of 21.5 mA cm^{-2} and an FF of 68.4%. Grazing incidence X-ray diffraction, atomic force microscopy and scanning electron microscopy indicated a nanofibril-type crystallinity for the **PK9** film, which seems to result in better charge mobility.[172]

A further study of interest was published by Molina *et al.*, who reported four ZnPc dimers with 2,5-thienyl (**PKB**), 2,7-fluorenyl (**PKC**), 3,6-bisthienyldiketopyrrolopyrrole (**BH36**)[82] and 1,4-phenyl (**PKD**)[173] bridges as dopant-free HTMs in a triple-cation system $[Cs_{0.05}(FA_{0.83}MA_{0.17})_{0.95}]Pb(I_{0.83}Br_{0.17})_3$ PSCs (Fig. 22c and Table 7). The push–pull character of **BH36** was found to confer a better performance on the PSC compared to the other dopant-free HTM systems studied, with a maximum PCE of 16.8%, a J_{sc} of 20.6 mA cm^{-2}, a V_{oc} of 1.10 V and an FF of 73.8%, compared to PCEs of 15.5%, 15.6% and 15.7% for **PKB**, **PKC** and **PKD**, respectively, all of them measured under standard global AM 1.5 illumination. Steady-state and time-resolved photoluminescence studies suggested that these dopant-free materials had a comparable hole-extraction capacity to doped spiro-OMeTAD. Shelf and thermal stability tests showed that all ZnPc-based materials studied were more stable than doped spiro-OMeTAD.[174]

Four HTMs based on DPPs were compared in an interesting study that has been published very recently. The structures include a central DPP with two triphenylamine pendent groups linked to both thiophenes. The structural difference is the alkyl side-chain substituents (2-ethylhexyl-, *n*-hexyl-, ((methoxyethoxy) ethoxy)ethyl-, and (2-((2-methoxyethoxy)ethoxy)ethyl)acetamide, referred to here as **PK10**, **PK11**, **PK12** and **PK13**; Fig. 22d). **PK13** gave the best results, exhibiting an efficiency of 17.64% as dopant-free HTM and exceeding 20% when LI-TFSI was added as a dopant (J_{sc} = 22.94 mA cm^{-2}, V_{oc} = 1.14 V, FF = 73.87%; see Table 7).[175]

4.2. DPP-based single molecules with other roles in PSCs

Different DPP derivatives have also been investigated in other roles within PSC devices, for example as ETMs, additives and interlayers. Thus, Patil *et al.* published a study in which the performance of p–i–n planar PSC devices containing **PK14** or PCMB, or a mixture of both, as ETL, and with different perovskite compositions, are compared. **PK14** (Fig. 23a) has a simple quinoidal structure possessing terminal malononitrile groups. These authors obtained a discrete 3.57% PCE with the double-cation $FA_{0.85}MA_{0.15}Pb(I_{0.8}Br_{0.2})_3$ perovskite composition when **PK14** was the ETL. Although PCBM was better than **PK14** in terms of photovoltaic performance (PCE = 8.82%), **PK14** offers greater stability than PCBM in OFETs under ambient conditions.[176] Huang *et al.* used the molecule **PK15** as a 3D additive in perovskite films (Fig. 23c), adding 0, 0.01 and 0.02 wt% **PK15** to the $MAPbI_3$ perovskite solution during manufacture of the devices. Those devices containing 0.01 wt% **PK15** in the perovskite layer gave a better performance, with a J_{sc} of 21.04 mA cm^{-2}, a V_{oc} of 1.02 V, an FF of 65.9% and a PCE of 14.1%, compared to PCEs of 10.6% and 11.6% when 0% and 0.02 wt% of **PK15**, respectively, was added. X-ray diffraction and scanning electron microscopy studies showed that **PK15** acts as a crystallinity improver and grain-boundary filler, UV-vis spectroscopy studies showed that it acts as a light-capturer, and cyclic voltammetry, steady-state and time resolved photoluminescence

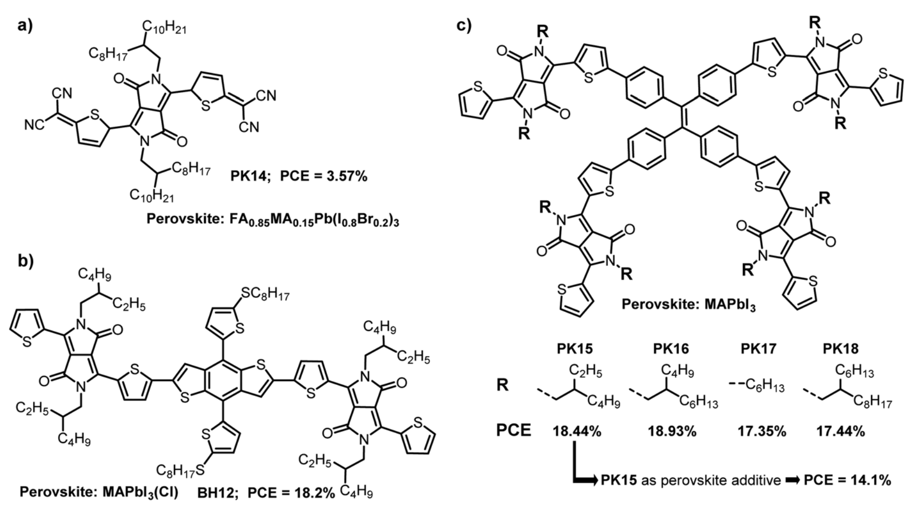

Fig. 23 Chemical structures and PCEs for **PK14–PK18**. Perovskite compositions are included.

analysis showed that it also acts as additional electron-donor.[177] Zhang *et al.* were the first to use a p-type organic semiconductor (**BH12**, Fig. 23b) as the interlayer at a perovskite/HTL interface in n–i–p PSCs, thereby improving the efficiency and stability. **BH12** is based on benzo[1,2-*b*:4,5-*b*′]dithiophene flanked with two diketopyrrolopyrrole units. PSCs with a **BH12** interlayer showed better performances, with a J_{sc} of 22.0 mA cm^{-2}, a V_{oc} of 1.06 V, an FF of 77.9% and a PCE of 18.2%, compared to a PCE of 16.9% for the control devices. High hole mobility and an appropriate energy level alignment to $MAPbI_3$(Cl) were found. The numerous sulfur atoms can act as Lewis bases, passivating the perovskite layer surface by forming Lewis adducts between infra-coordinated Pb and S, as confirmed by Fourier-transform infrared and Raman spectroscopy; the energy profile was confirmed by performing trap density-of-states measurements. Devices with a **BH12** interlayer exhibited greater stability under ambient conditions during 7 days than control devices due to the hydrophobic nature of **BH12**, which protects the perovskite layer from moisture.[178] Derivatives **PK15**, **PK16**, **PK17** and **PK18** were also used as an interlayer between the perovskite layer and the ETL C_{60} in planar p–i–n PSCs with an $MAPbI_3$ perovskite composition (Fig. 23c). The chemical structures are tetraphenylethylene-diketopyrrolopyrrole with different branched *N*-alkyl chain lengths. The authors demonstrated that the length of the *N*-alkyl chain leads to different surface morphologies in the solid state, thus meaning that the ability to extract electrons is affected. All the devices with a DPP-interlayer exhibited a better performance than those with no interlayer, especially those containing **PK16**, which exhibited a maximum PCE of 18.93%, a V_{oc} of 1.06 V, a J_{sc} of 22.47 mA cm^{-2} and a high FF of 80%. The maximum PCEs for the devices using **PK15**, **PK17** and **PK18** interlayers were 18.44%, 17.35%, and 17.44%, respectively.[179,180]

In summary, considering the state of the art (PCE > 25%), there is still significant scope for improvement in DPP-based HTM designs. Moreover, features such as hydrophobicity, synthetic versatility, and robustness, along with existing industrial DPP-pigment development, should encourage researchers to find cheap-to-produce DPP-based molecules for PSC applications.

5. Outlook and conclusions

In this article we have reviewed the most relevant studies in the field of photovoltaics involving DPP-based single molecules from the last few years. We have provided a perspective based on the chemical structure in an attempt to find clues about its relationship to performance. DPP-based single molecules stand out as donors in BHJ OSCs, with the highest efficiencies for single-molecule-based devices of more than 12%. The push–pull character of the molecules, in which the acceptor character of the DPP-core and the donor character of other units act together, is decisive for the effective self-ordering of the molecules in the solid state, especially with the appropriate annealing and doping treatments. The molecular design strategies that stand out to date are extension of the conjugation using ethynyl connectors between the different units that make up the molecule, as well as the inclusion of porphyrinoids in the molecular structure in the case of donor systems. DPP-based single molecules are also promising acceptors in OCSs since their chemical versatility allows the energy levels of the acceptor materials to be tuned and to compete with the FA. In general, although star-shaped NFA designs lead to a better performance for OPV devices, a linear donor molecule with a DPP core currently holds the record of 10.05% PCE. Varying results have been obtained for DSSCs to date, probably due to the tendency of DPP derivatives to aggregate, which increases the probability of charge recombination. As such, it is necessary to design structures in which there is a compromise between the tendency to aggregate and adequate charge conduction. As for as the most popular experimental photovoltaic technology to date, namely perovskite solar cells, is concerned, DPP single molecules cannot currently compete with reference materials (*e.g.* spiro-OMeTAD and PTAA) in terms of efficiency, although they are similar in terms of stability. In addition, it must be considered that the number of publications in each field is currently very different. Even so, a promising maximum PCE of more than 20% has been obtained with the HTM **PK13**. Furthermore, when included in other roles, for example as ETLs, interlayers or perovskite additives, some benefit has generally been obtained, mainly an improvement in PV parameters and/or stability. These push–pull systems may prove to be fundamental for the development of materials with the characteristics needed for indoor and outdoor PV applications.

Conflicts of interest

There are no conflicts to declare.

Acknowledgements

ASS thanks the Spanish Ministerio de Ciencia e Innovación (MICINN/FEDER) for financial support (CTQ2017-87102-R). MJAM thanks ''Beca Santiago Grisolia Grisoliap20177153'' de la Comunidad Valenciana.

References

1 A. Mahmood, J.-Y. Hu, B. Xiao, A. Tang, X. Wang and E. Zhou, *J. Mater. Chem. A*, 2018, **6**, 16769.
2 Ö. Birel, S. Nadeem and H. Duman, *J. Fluoresc.*, 2017, **27**, 1075.
3 M. Urbani, M.-E. Ragoussi, M. K. Nazeeruddin and T. Torres, *Coord. Chem. Rev.*, 2019, **381**, 1.
4 Y. Duan, X. Xu, Y. Li and Q. Peng, *Chin. Chem. Lett.*, 2017, **28**, 2105.
5 F. Fernández-Lázaro, N. Zink-Lorre and Á. Sastre-Santos, *J. Mater. Chem. A*, 2016, **4**, 9336.
6 A. Tang, C. Zhan, J. Yao and E. Zhou, *Adv. Mater.*, 2017, **29**, 1600013.
7 M. Kaur and D. H. Cho, *Chem. Soc. Rev.*, 2015, **44**, 58.
8 Q. Liu, S. E. Bottle and P. Sonar, *Adv. Mater.*, 2019, 1903882.

9 W. Li, K. H. Hendriks, M. M. Wienk and R. A. J. Janssen, *Acc. Chem. Res.*, 2016, **49**, 78.
10 Y. Patil and R. Misra, *Chem. – Asian J.*, 2018, **13**, 220.
11 D. G. Farnum, G. Mehta, G. G. I. Moore and F. P. Siegal, *Tetrahedron Lett.*, 1974, **15**, 2549.
12 Z. Hao and A. Iqbal, *Chem. Soc. Rev.*, 1997, **26**, 203.
13 S. Ghosh, S. Shankar, D. S. Philips and A. Ajayaghosh, *Mater. Today Chem.*, 2020, **16**, 100242.
14 A. Iqbal and L. Cassar, *EP 98808*, 1984 *; Chem. Abstr.*, 1984, **100**, 176461.
15 S. Loser, S. J. Lou, B. M. Savoie, C. J. Bruns, A. Timalsina, M. J. Leonardi, J. N. Smith, T. Harschneck, R. Turrisi, N. Zhou, C. L. Stern, A. A. Sarjeant, A. Facchetti, R. P. H. Chang, S. I. Stupp, M. A. Ratner, L. X. Chen and T. J. Marks, *J. Mater. Chem. A*, 2017, **5**, 9217.
16 Y. Patil and R. Misra, *J. Mater. Chem. C*, 2019, **7**, 13020.
17 M. Grzybowski and D. T. Gryko, *Adv. Opt. Mater.*, 2015, **3**, 280–320.
18 S. Qu and H. Tian, *Chem. Commun.*, 2012, **48**, 3039.
19 G. Zhang, Y. Fu, Z. Xie and Q. Zhang, *Sol. Energy Mater. Sol. Cells*, 2011, **85**, 1168.
20 T. K. An, I. Kang, H.-J. Yun, H. Cha, J. Hwang, S. Park, J. Kim, Y. J. Kim, D. S. Chung, S.-K. Kwon, Y.-H. Kim and C. E. Park, *Adv. Mater.*, 2013, **25**, 7003.
21 G.-S. Ryu, K. H. Park, W.-T. Park, Y.-H. Kim and Y.-Y. Noh, *Org. Electron.*, 2015, **23**, 76.
22 Y. Li, P. Sonar, L. Murphya and W. Hong, *Energy Environ. Sci.*, 2013, **6**, 1684.
23 Y. Tan, L. Chen, F. Wu, B. Huang, Z. Liao, Z. Yu, L. Hu, Y. Zhou and Y. Chen, *Macromolecules*, 2018, **51**, 8197.
24 J. Huang, C. Zhan, X. Zhang, Y. Zhao, Z. Lu, H. Jia, B. Jiang, J. Ye, S. Zhang, A. Tang, Y. Liu, Q. Pei and J. Yao, *Appl. Mater. Interfaces*, 2013, **5**, 2033.
25 P. Sonar, T. R. B. Foonga and A. Dodabalapur, *Phys. Chem. Chem. Phys.*, 2014, **16**, 4275.
26 Z. Jiang, Z. Ni, H. Wang, Z. Wang, J. Zhang, G. Qiu, J. Fang, Y. Zhang, H. Dong, K. Lu, W. Hu and Z. Wei, *Polym. Chem.*, 2017, **8**, 5603.
27 B. Lim, H. Sun, J. Lee and Y.-Y. Noh, *Sci. Rep.*, 2017, **7**, 164.
28 Y. Qu, Y. Wu, Y. Gao, S. Qu, L. Yang and J. Hua, *Sens. Actuators, B*, 2014, **197**, 13.
29 S. G. Suryaa, S. S. Nagarkar, S. K. Ghoshc, P. Sonar and V. R. Rao, *Sens. Actuators, B*, 2016, **223**, 114.
30 S. Zhang, T. Sun, D. Xiao, F. Yuan, T. Li, E. Wang, H. Liu and Q. Niu, *Spectrochim. Acta, Part A*, 2018, **189**, 594.
31 L. Wang, L. Yang, L. Huang and D. Cao, *Sens. Actuators, B*, 2015, **209**, 536.
32 M. Kaur and D. H. Choi, *Sens. Actuators, B*, 2014, **190**, 542.
33 M. R. Kaur, D. S. Yang, K. Choi, M. J. Cho and D. H. Choi, *Dyes Pigm.*, 2014, **100**, 118.
34 X. Yang, X. Liu, Y. Li, F. Wu, J. Mao, Y. Yuan, Y. Cui, G. Sun and G. Zhang, *Biosens. Bioelectron.*, 2016, **80**, 288.
35 T. Mukhopadhyay, A. J. Musser, B. Puttaraju, J. Dhar, R. H. Friend and S. Patil, *J. Phys. Chem. Lett.*, 2017, **8**, 984.
36 I. Papadopoulos, M. J. Álvaro-Martins, D. Molina, P. M. McCosker, P. A. Keller, T. Clark, Á. Sastre-Santos and D. M. Guldi, *Adv. Energy Mater.*, 2020, 2001496.
37 C. B. Nielsen, M. Turbiez and L. McCulloch, *Adv. Mater.*, 2013, **25**, 1859.
38 S. D. Collins, N. A. Ran, M. C. Heiber and T.-Q. Nguyen, *Adv. Energy Mater.*, 2017, **7**, 1602242.
39 Z. Wang, L. Zhu, Z. Shuai and Z. Wei, *Macromol. Rapid Commun.*, 2017, **38**, 1700470.
40 P. Cheng, G. Li, X. Zhan and Y. Yang, *Nat. Photonic.*, 2018, **12**, 131–142.
41 B. C. Thompson and J. M. J. Fréchet, *Angew. Chem., Int. Ed.*, 2008, **47**, 58–77.
42 A. Facchetti, *Mater. Today*, 2013, **16**, 123–132.
43 A. C. Mayer, S. R. Scully, B. E. Hardin, M. W. Rowell and M. D. McGehee, *Mater. Today*, 2007, **10**, 28–33.
44 M. K. Siddiki, J. Li, D. Galipeau and Q. Qiao, *Energy Environ. Sci.*, 2010, **3**, 867–883.
45 S. Rafiquea, S. M. Abdullaha, K. Sulaimana and M. Iwamotob, *Renewable Sustainable Energy Rev.*, 2018, **84**, 43–53.
46 C. Yan, S. Barlow, Z. Wang, H. Yan, A. K.-Y. Jen, S. R. Marder and X. Zhan, *Nat. Rev. Mater*, 2018, **3**, 18003.
47 G. Li, D. Li, R. Ma, T. Liu, Z. Luo, G. I. Cui, L. Tong, M. Zhang, Z. Wang, F. Liu, L. Xu, H. Yan and B. Tang, *J. Mater. Chem. A*, 2020, **8**, 5927–5935.
48 https://www.nrel.gov/pv/cell-efficiency.html accessed 2021/05/24.
49 M. Green, E. Dunlop, J. Hohl-Ebinger, M. Yoshita, N. Kopidakis and X. Hao, *Prog. Photovolt. Res. Appl.*, 2021, **29**, 3–15.
50 C. W. Tang, *Appl. Phys. Lett.*, 1986, **48**, 2.
51 D. Kekuda, J.-S. Huang, M. Velusamy, J. T. Lin and C.-W. Chu, *Sol. Energy Mater. Sol. Cells*, 2010, **94**, 1767–1771.
52 C. W. Tang, *Appl. Phys. Lett.*, 1986, **48**, 183.
53 W. Kylberg, P. Sonar, J. Heier, J.-N. Tisserant, C. Muller, F. Nuesch, Z.-K. Chen, A. Dodabalapur, S. Yoon and R. Hany, *Energy Environ. Sci.*, 2011, **4**, 3617.
54 P. Sonar, G.-M. Ng, T. T. Lin, A. Dodabalapur and Z.-K. Chen, *J. Mater. Chem.*, 2010, **20**, 3626–3636.
55 Y. Peng, L. Zhang and T. L. Andrew, *Appl. Phys. Lett.*, 2014, **105**, 083304.
56 J. S. Zambounis, Z. Hao and A. Iqbal, *Nature*, 1997, **388**, 131–132.
57 M. Rooney, F. Carulli, S. Luzzati, R. Resel, B. Schrode, R. Ruffo, M. Sassi and L. Beverina, *Org. Photonics Photovolt*, 2018, **6**, 8–16.
58 H. Meier, *Angew. Chem., Int. Ed.*, 2005, **44**, 2482–2506.
59 Y. Patil, R. Misra, F. C. Chen, M. L. Keshtov and G. D. Sharma, *RSC Adv.*, 2016, **6**, 99685–99694.
60 Y. Patil, R. Misra, F. C. Chen and G. D. Sharma, *Phys. Chem. Chem. Phys.*, 2016, **18**, 22999–23005.
61 Y. Patil, R. Misra, M. K. Singh and G. D. Sharma, *Phys. Chem. Chem. Phys.*, 2017, **19**, 7262–7269.
62 H.-J. Yun, H. H. Choi, S.-K. Kwon, Y.-H. Kim and K. Cho, *Chem. Mater.*, 2014, **26**, 3928–3937.

63 H. Shi, W. Fu, M. Shi, J. Ling and H. Chen, *J. Mater. Chem. A*, 2015, **3**, 1902.
64 J. W. Jung, T. P. Russell and W. H. Jo, *Chem. Mater.*, 2015, **27**, 4865–4870.
65 Z. Tang, B. Liu, A. Melianas, J. Bergqvist, W. Tress, Q. Bao, D. Qian, O. Inganäs and F. Zhang, *Adv. Mater.*, 2015, **27**, 1900–1907.
66 G. Feng, Y. Xu, J. Zhang, Z. Wang, Y. Zhou, Y. Li, Z. Wei and C. L. W. Li, *J. Mater. Chem. A*, 2016, **4**, 6056–6063.
67 Y. Patil, R. Misra, A. Sharma and G. D. Sharma, *Phys. Chem. Chem. Phys.*, 2016, **18**, 16950–16957.
68 Y. Lin, J. Wang, T. Li, Y. Wu, C. Wang, L. Han, Y. Yao, W. Ma and X. Zhan, *J. Mater. Chem. A*, 2016, **4**, 1486–1494.
69 Y. Huo, J. Zhu, X.-Z. Wang, C. Yan, Y.-F. Chai, Z.-Z. Chen, X. Zhan and H.-L. Zhang, *J. Mater. Chem. C*, 2018, **6**, 5843–5848.
70 W. Leea, J. Choib and J. W. Jung, *Dyes Pigm.*, 2019, **161**, 283–287.
71 A. L. Kanibolotsky, I. F. Perepichka and P. J. Skabara, *Chem. Soc. Rev.*, 2010, **39**, 2695–2728.
72 S.-Y. Shiau, C.-H. Chang, W.-J. Chen, H.-J. Wang, R.-J. Jeng and R.-H. Lee, *Dyes Pigm.*, 2015, **115**, 35–49.
73 S.-Y. Liu, J. W. Jung, C.-Z. Li, J. Huang, J. Zhang, H. Chen and A. K.-Y. Jen, *J. Mater. Chem. A*, 2015, **3**, 22162–22169.
74 J. Min-Park, J. H. Lee and W. D. Jang, *Coord. Chem. Rev.*, 2020, **407**, 213157.
75 H. M. Qin, L. S. Li, F. Q. Guo, S. J. Su, J. B. Peng, Y. Cao and X. B. Peng, *Energy Environ. Sci.*, 2014, **7**, 1397–1401.
76 T. Liang, L. Xiao, C. Liu, K. Gao, H. Qin, Y. Cao and X. Peng, *Org. Electron.*, 2016, **29**, 127–134.
77 L. Bucher, N. Desbois, E. L. N. Koukaras, C. H. Devillers, S. Biswas, G. D. Sharma and C. P. Gros, *J. Mater. Chem. A*, 2018, **6**, 8449–8461.
78 W. T. Hadmojo, D. Yim, S. Sinaga, W. Lee, D. Y. Ryu, W.-D. Jang, I. H. Jung and S.-Y. Jang, *ACS Sustainable Chem. Eng.*, 2018, **6**, 5306–5313.
79 K. Gao, J. Miao, L. Xiao, W. Deng, Y. Kan, T. Liang, C. Wang, F. Huang, J. Peng, Y. Cao, F. Liu, T. P. Russell, H. Wu and X. Peng, *Adv. Mater.*, 2016, **28**, 4727–4733.
80 X. Shi, J. Chen, K. Gao, L. Zuo, Z. Yao, F. Liu, J. Tang and A. K.-Y. Jen, *Adv. Energy Mater.*, 2018, **8**, 1702831.
81 K. Gao, S. B. Jo, X. Shi, L. Nian, M. Zhang, Y. Kan, F. Lin, B. Kan, B. Xu, Q. Rong, L. Shui, F. Liu, X. Peng, G. Zhou, Y. Cao and A. K.-Y. Jen, *Adv. Mater.*, 2019, **31**, 1807842.
82 V. Cuesta, M. Vartanian, P. Malhotra, S. Biswas, P. D. L. Cruz, G. D. Sharma and F. Langa, *J. Mater. Chem. A*, 2019, **7**, 11886–11894.
83 H.-H. Gao, Y. Sun, S. Li, X. Ke, Y. Cai, X. Wan, H. Zhang, C. Li and Y. Chen, *Dyes Pigm.*, 2020, **176**, 108250.
84 X. Gao, Y. Wu, X. Song, X. Tao, Y. He, T. Yang, R. Yu, Z. Li and Y. Tao, *Dyes Pigm.*, 2021, **188**, 109216.
85 D. Molina, A. Guerrero, G. Garcia-Belmonte, F. Fernández-Lázaro and A. Sastre-Santos, *Eur. J. Org. Chem.*, 2014, 4585.
86 P. Sonar, G.-M. Ng, T. T. Lin, A. Dodabalapur and Z.-K. Chen, *J. Mater. Chem.*, 2010, **20**, 3626–3636.
87 B. P. Karsten, J. C. Bijleveld and R. A. Janssen, *Rapid Commun.*, 2010, **31**, 1554–1559.
88 Y. Patil, R. Misra, M. L. Keshtov and G. D. Sharma, *J. Phys. Chem. C*, 2016, **120**, 6324–6335.
89 Y. Patil, T. Jadhav, B. Dhokale and R. Misra, *Asian J. Org. Chem.*, 2016, **5**, 1008–1010.
90 Y. Patil, R. Misraa, M. L. Keshtov and G. D. Sharma, *J. Mater. Chem. A*, 2017, **5**, 3311–3319.
91 Y. Patila, R. Misraa, R. Singhalb and G. D. Sharma, *J. Mater. Chem. A*, 2017, **5**, 13625–13633.
92 P. Josse, C. Dalinot, Y. Jiang, S. D. Seignon, J. Roncali, P. Blanchard and C. Cabanetos, *J. Mater. Chem. A*, 2016, **4**, 250–256.
93 P. Josse, A. Labrunie, C. Dalinot, S. M. McAfee, S. D. Seignon, J. Roncali, G. C. Welch, P. Blanchard and C. Cabanetos, *Org. Electron.*, 2016, **37**, 479–484.
94 Y. Eom, C. E. Song, W. S. Shin, S. K. Lee and E. Lim, *J. Ind. Eng. Chem.*, 2017, **45**, 338–348.
95 M. Privado, V. Cuesta, P. D. L. Cruz, M. L. Keshtov, R. Singhal, G. D. Sharma and F. Langa, *ACS Appl. Mater. Interfaces*, 2017, **9**, 11739–11748.
96 Y. Eom, C. E. Song, W. S. Shin, S. K. Lee and E. Lim, *J. Ind. Eng. Chem.*, 2017, **45**, 338–348.
97 M. Privado, V. Cuesta, P. D. L. Cruz, M. L. Keshtov, G. D. Sharma and F. Langa, *J. Mater. Chem. A*, 2017, **5**, 14259–14269.
98 M. Privado, P. D. L. Cruz, S. Biswas, R. Singhal, G. D. Sharma and F. Langa, *J. Mater. Chem. A*, 2018, **6**, 11714–11724.
99 S. M. McAfee, S. V. Dayneko, P. Josse, P. Blanchard, C. Cabanetos and G. C. Welch, *Chem. Mater.*, 2017, **29**, 1309–1314.
100 S. M. McAfee, A.-J. Payne, S. V. Dayneko, G. P. Kini, C. E. Song, J.-C. Lee and G. C. Welch, *J. Mater. Chem. A*, 2017, **5**, 16907–16913.
101 M. Privado, P. Malhotra, P. de la Cruz, R. Singhal, J. Cerdá, J. Aragó, E. Ortí, G. D. Sharma and F. Langa, *Sol. RRL*, 2020, **4**, 1900471.
102 S. Li, J. Yan, C.-Z. Li, F. Liu, M. Shi, H. Chen and T. P. Russell, *J. Mater. Chem. A*, 2016, **4**, 3777–3783.
103 A. M. Raynor, A. Gupta, H. Patil, D. Ma, A. Bilic, T. Rooka and S. V. Bhosale, *RSC Adv.*, 2016, **6**, 28103–28109.
104 J. W. Jung and W. H. Jo, *Chem. Mater.*, 2015, **27**, 6038–6043.
105 Y.-Q. Pan and G.-Y. Sun, *ChemSusChem*, 2019, **12**, 4570.
106 X. Huang, M. Hu, X. Zhao, C. Li, Z. Yuan, X. Liu, C. Cai, Y. Zhang, Y. Hu and Y. Chen, *Org. Lett.*, 2019, **21**, 3382.
107 H. Hang, X. Wu, Q. Xu, Y. Chen, H. Li, W. Wang, H. Tong and L. Wang, *Dyes Pigm.*, 2019, **160**, 243.
108 Y. N. Luponosov, A. N. Solodukhin, A. L. Mannanov, P. S. Savchenko, Y. Minenkov, D. Y. Paraschuk and S. A. Ponomarenko, *Dyes Pigm.*, 2020, **177**, 108260.
109 K. Wang, P. Xia, K. Wang, X. You, M. Wu, H. Huang, D. Wu and J. Xia, *ACS Appl. Mater. Interfaces*, 2020, **12**, 9528.
110 A. Stanculescua, C. Breazua, M. Socol, O. Rasoga, N. Preda, G. Petre, A. M. Solonaru, M. Grigoras, F. Stanculescu, G. Socol, G. Popescu-Pelin and M. Girtan, *Appl. Surf. Sci.*, 2020, **509**, 145351.

111 J. Hu, X. Liu, K. Wang, M. Wu, H. Huang, D. Wu and J. Xia, *J. Mater. Chem. C*, 2020, **8**, 2135.
112 B. A. Gregg, *J. Phys. Chem. Lett.*, 2011, **2**, 3013.
113 C. Zhan, X. Zhang and J. Yao, *RSC Adv.*, 2015, **5**, 93002.
114 A. Gupta, A. Rananaware, P. S. Rao, D. D. La, A. Bilic, W. Xiang, J. Li, R. A. Evans, S. V. Bhosalec and S. V. Bhosale, *Mater. Chem. Front.*, 2017, **1**, 1600–1606.
115 A. Rananaware, A. Gupta, J. L. Li, A. Bilic, L. Jones, S. Bhargavad and S. V. Bhosale, *Chem. Commun.*, 2016, **52**, 8522–8525.
116 S.-Y. Liu, W.-Q. Liu, C.-X. Yuan, A.-G. Zhong, D. Han, B. Wang, M. N. Shah, M.-M. Shi and H. Chen, *Dyes Pigm.*, 2016, **134**, 139–147.
117 P. Sun, H. Sun, X. Li, Y. Wang, H. Shan, J. Xu, C. Zhang, Z. Xu, Z.-K. Chen and W. Huang, *Dyes Pigm.*, 2017, **139**, 412–419.
118 H. Yuhui, W. Wenlin, Y. Liyang, L. Kaijun, X. Xiaopeng, L. Ying and P. Qiang, *Acta Chim. Sin.*, 2020, **78**, 1246.
119 R. W. Jadhav, R. W. Hangarge, M. D. Aljabri, K. S. More, J.-Y. Chen, L. A. Jones, R. A. Evans, J.-L. Li, S. V. Bhosale and A. Gupta, *Mater. Chem. Front.*, 2020, **4**, 2176.
120 M. J. Álvaro-Martins, J. G. Sánchez, G. Lavarda, D. Molina, J. Pallarès, T. Torres, L. F. Marsal and Á. Sastre-Santos, *ChemPlusChem*, 2021, **86**, DOI: 10.1002/cplu.202100103.
121 X.-F. Wu, W.-F. Fu, Z. Xu, M. Shi, F. Liu, H.-Z. Chen, J.-H. Wan and T. P. Russell, *Adv. Funct. Mater.*, 2015, **25**, 5954–5966.
122 S. Li, W. Liu, M. Shi, J. Mai, T.-K. Lau, J. Wan, X. Lu, C.-Z. Li and H. Chen, *Energy Environ. Sci.*, 2016, **9**, 604–610.
123 W. Liu, S. Li, J. Huang, S. Yang, J. Chen, L. Zuo, M. Shi, X. Zhan, C.-Z. Li and H. Chen, *Adv. Mater.*, 2016, **28**, 9729–9734.
124 Z.-C. Chen, Y. Xie, Y.-Y. Yu, H.-B. Wu and J.-H. Wan, *New J. Chem.*, 2018, **42**, 11854–11861.
125 P. Sun, X. Li, Y. Wang, H. Shan, J. Xu, C. Liu, C. Zhang, F. Chen, Z. Xu, Z.-K. Chen and W. Huang, *RSC Adv.*, 2018, **8**, 25031–25039.
126 B. O'Regan and M. Grätzel, *Nature*, 1991, **353**, 737.
127 E. Benazzi, J. Mallows, G. H. Summers, F. A. Blacka and E. A. Gibson, *J. Mater. Chem. C*, 2019, **7**, 10409.
128 R. Cisneros, M. Beley and F. Lapicque, *Phys. Chem. Chem. Phys.*, 2016, **00**, 1.
129 H.-W. Bahng, A. Hagfeldt and J.-E. Moser, *J. Phys. Chem. C*, 2018, **122**, 19348.
130 H.-W. Bahng, A. Hagfeldt and J.-E. Moser, *J. Phys. Chem. C*, 2018, **122**, 19359.
131 S. Mathew, A. Yella, P. Gao, R. Humphry-Baker, B. F. Curchod, N. Ashari-Astani, I. Tavernelli, U. Rothlisberger, M. K. Nazeeruddin and M. Gratzel, *Nat. Chem.*, 2014, **6**, 242.
132 Y. Lu, Y. Cheng, C. Li, J. Luo, W. Tang, S. Zhao, Q. Liu and Y. Xie, *Sci. China: Chem.*, 2019, **62**, 994.
133 D. Zhang, M. Stojanovic, Y. Ren, Y. Cao, F. T. Eickemeyer, E. Socie, N. Vlachopoulos, J.-E. Moser, S. M. Zakeeruddin, A. Hagfeldt and M. Grätzel, *Nat. Commun.*, 2021, **12**, 1777.
134 K. Kunimoto, H. Yamamoto, S. Nakamichi, R. Takahashi and J. Tanabe, *PCT Int. Appl.* (2009), WO 2009109499 A1 20090911.
135 F.-L. Guo, S.-Y. Qu, W.-J. Wu, J. Li, W.-J. Ying and J.-L. Hua, *Synth. Met.*, 2010, **160**, 1767.
136 S. Qu, W. Wu, J. Hua, C. Kong, Y. Long and H. Tian, *J. Phys. Chem.*, 2010, **114**, 1343.
137 F. Guo, X. Liu, Y. Ding, F. Kong, W. Chen, L. Zhoua and S. Dai, *RSC Adv.*, 2016, **6**, 13433.
138 J. Zhang, N. Vlachopoulos, Y. Hao, T. W. Holcombe, G. Boschloo, E. M. J. Johansson, M. Grätzel and A. Hagfeldt, *Chem. Phys. Chem.*, 2016, **17**, 1441.
139 Z. Liu, K. Duan, H. Guo, Y. Deng, H. Huang, X. Yi, H. Chen and S. Tan, *Dyes Pigm.*, 2017, **140**, 312.
140 A. E. Yemene, V. Venkatraman, D. M. Almenningen, B. H. Hoff and O. R. Gautun, *Molecules*, 2020, **25**, 2349.
141 J.-H. Yum, T. W. Holcombe, Y. Kim, K. Rakstys, T. Moehl, J. Teuscher, J. H. Delcamp, M. K. Nazeeruddin and M. Grätzel, *Sci. Rep.*, 2013, **3**, 2446.
142 P. Ganesan, A. Yella, T. W. Holcombe, P. Gao, R. Rajalingam, S. A. Al-Muhtaseb, M. Grätzel and M. K. Nazeeruddin, *ACS Sustainable Chem. Eng.*, 2015, **3**, 2389.
143 X. Li, Z. Zheng, W. Jiang, W. Wu, Z. Wang and H. Tian, *Chem. Commun.*, 2015, **51**, 3590.
144 K. Y. Chiu, V. Govindan, L.-C. Lin, S.-H. Huang, J.-C. Hu, K.-M. Lee, H.-H. G. Tsai, S.-H. Chang and C.-G. Wu, *Dyes Pigm.*, 2016, **125**, 27.
145 Y. Hao, Y. Saygili, J. Cong, A. Eriksson, W. Yang, J. Zhang, E. Polanski, K. Nonomura, S. M. Zakeeruddin, M. Grätzel, A. Hagfeldt and G. Boschloo, *ACS Appl. Mater. Interfaces*, 2016, **8**, 32797.
146 H. Shimogawa, M. Endo, T. Taniguchi, Y. Nakaike, M. Kawaraya, H. Segawa, Y. Murata and A. Wakamiya, *Bull. Chem. Soc. Jpn.*, 2017, **90**, 441.
147 H. Shimogawa, M. Endo, Y. Nakaike, Y. Murata and A. Wakamiya, *Chem. Lett.*, 2017, **46**, 715.
148 S. Zhang, X. Yang, C. Qin, Y. Numata and L. Han, *J. Mater. Chem. A*, 2014, **2**, 5167.
149 G. Boschloo, L. Häggman and A. Hagfeldt, *J. Phys. Chem. B*, 2006, **110**, 13144.
150 G. Wang, Z. Liu, Y. Deng, L. Xie and S. Tan, *Dyes Pigm.*, 2017, **145**, 427.
151 J.-D. Decoppet, S. B. Khan, M. S. A. Al-Ghamdi, B. G. Alhogbi, A. M. Asiri, S. M. Zakeeruddin and M. Grätzel, *Energy Technol.*, 2017, **5**, 321.
152 D.-S. Lim, K. Choi, D. Hayati, D.-H. Park, A. Ghifari, K. M. Lee, Y. Ko, Y. Jun, H.-J. Suk and J. Hong, *Dyes Pigm.*, 2020, **173**, 107840.
153 I. R. Perera, T. Daeneke, S. Makuta, Z. Yu, Y. Tachibana, A. Mishra, P. Buerle, C. A. Ohlin, U. Bach and L. Spiccia, *Angew. Chem., Int. Ed.*, 2015, **54**, 3758.
154 L. Favereau, J. Warnan, Y. Pellegrin, E. Blart, M. Boujtita, D. Jacquemin and F. Odobel, *Chem. Commun.*, 2013, **49**, 8018.
155 Y. Farré, L. Zhang, Y. Pellegrin, A. Planchat, E. Blart, M. Boujtita, L. Hammarström, D. Jacquemin and F. Odobel, *J. Phys. Chem. C*, 2016, **120**, 7923.

156 Y. Farré, M. Raissi, A. Fihey, Y. Pellegrin, E. Blart, D. Jacquemin and F. Odobel, *ChemSusChem*, 2017, **10**, 2618–2625.
157 T. T. T. Pham, S. K. Saha, D. Provost, Y. Farré, M. Raissi, Y. Pellegrin, E. Blart, S. Vedraine, B. Ratier, D. Aldakov, F. Odobel and J. Bouclé, *J. Phys. Chem. C*, 2017, **121**, 129.
158 L. Zhang, G. Boschloo, L. Hammarströma and H. Tian, *Phys. Chem. Chem. Phys.*, 2016, **18**, 5080.
159 N. G. Park, M. Grätzel and T. Miyasaka, *Organic–inorganic halide perovskite photovoltaics: From fundamentals to device architectures*, Springer International Publishing, 2016, pp. 1–366, ISBN 978-3-319-35114-8.
160 https://www.nrel.gov/pv/assets/pdfs/best-research-cell-efficiencies.20190802.pdf, accessed 2021/05/24.
161 M. I. H. Ansari, A. Qurashi and M. K. Nazeeruddin, *J. Photochem. Photobiol., C*, 2018, **35**, 1.
162 Z. Yang, J. Song, H. Zeng and M. Wang, *Mater. Today Energy*, 2019, **14**, 100338.
163 W.-W. Liu, T.-H. Wu, M.-C. Liu, W.-J. Niu and Y.-L. Chueh, *Adv. Mater. Interfaces*, 2019, **6**, 1801758.
164 J.-Y. Seo, H.-S. Kim, S. Akin, M. Stojanovic, E. Simon, M. Fleischer, A. Hagfeldt, S. M. Zakeeruddin and M. Grätzel, *Energy Environ. Sci.*, 2018, **11**, 2985.
165 J. Luo, C. Jia, Z. Wan, F. Han, B. Zhao and R. Wang, *J. Power Sources*, 2017, **342**, 886.
166 B. Xu, J. Huang, H. Agren, L. Kloo, A. Hagfeldt and L. Sun, *ChemSusChem*, 2014, **7**, 3252.
167 A. Tang, C. Zhan, J. Yao and E. Zhou, *Adv. Mater.*, 2017, **29**, 1600013.
168 Y. Patil and R. Misra, *Chem. – Asian J.*, 2018, **13**, 220.
169 S. Jeon, U. K. Thakur, D. Lee, Y. Wenping, D. Kim, S. Lee, T. K. Ahn, H. J. Park and B.-G. Kim, *Org. Electron.*, 2016, **37**, 134.
170 X. Liu, F. Kong, Z. Tan, T. Cheng, W. Chen, T. Yu, F. Guo, J. Chen, J. Yao and S. Dai, *RSC Adv.*, 2016, **6**, 87454.
171 H. Cheng, X. Zhao, Y. Shen, M. Wang, L. Wang, H. Meier and D. Cao, *J. Energy Chem.*, 2018, **27**, 1175.
172 S. R. Suranagi, R. Singh and M. Kim, *Dyes Pigm.*, 2019, **163**, 525.
173 D. Molina, M. A. Ruiz-Preciado, F. Sadegh, M. João Álvaro-Martins, M. Grätzel, A. Hagfeldt and Á. Sastre-Santos, *J. Porphyrins Phthalocyanines*, 2019, **23**, 547.
174 D. Molina, M. A. Ruiz-Preciado, B. Carlsen, F. T. Eickemeyer, B. Yang, M. J. Álvaro-Martins, K. Nonomura, A. Hagfeldt and Á. Sastre-Santos, *ChemPhotoChem*, 2020, **4**, 1.
175 A. Sharma, R. Singh, G. P. Kini, J. H. Kim, M. Parashar, M. Kim, M. Kumar, J. S. Kim and J.-J. Lee, *ACS Appl. Mater. Interfaces*, 2021, **13**, 7405.
176 S. Sharma, N. Sakai, S. Ray, Sa. P. Senanayak, H. Sirringhaus, H. J. Snaith and S. Patil, *Sol. Energy*, 2019, **186**, 9.
177 B. Huang, Q. Fu, Q. Ai, L. Tan, L. Chen and Y. Chen, *Mater. Chem. Front.*, 2017, **1**, 1179.
178 M. Zhang, J. Wang, L. Li, G. Zheng, K. Liu, M. Qin, H. Zhou and X. Zhan, *Adv. Sci.*, 2017, **4**, 1700025.
179 R. Wang, J. Qiao, B. He, X. Tang, F. Wu and L. Zhu, *J. Mater. Chem. C*, 2018, **6**, 8429.
180 B. He, R. Wang, H. Lu, Y. Ji, Q. Song, X. Tang, Y. Jin, F. Wu and L. Zhu, *Org. Electron.*, 2019, **69**, 13.